Henning Hvål Mathisen

# Experimental design and testing of a PCM-based heat storage unit for wood stoves

Master's thesis in Mechanical Engineering
Supervisor: Erling Næss, Alexis Sevault
September 2019

Master's thesis

NTNU
Norwegian University of Science and Technology
Faculty of Engineering
Department of Energy and Process Engineering

NTNU
Norwegian University of
Science and Technology

Henning Hvål Mathisen

# Experimental design and testing of a PCM-based heat storage unit for wood stoves

Master's thesis in Mechanical Engineering
Supervisor: Erling Næss, Alexis Sevault
September 2019

Norwegian University of Science and Technology
Faculty of Engineering
Department of Energy and Process Engineering

NTNU
Norwegian University of
Science and Technology

# Preface

This report presents my Master thesis (course TEP 4905) at the Department of Energy and Process Engineering (EPT), NTNU. The work has been carried out during the spring semester 2019 and was extended through the summer due to delays in the laboratory and difficulties with my computer.

To read the report, some knowledge of heat transfer is recommended.

I would like to thank my supervisors, Professor Erling Næss (EPT) and Research scientist Alexis Sevault (SINTEF Energy Research), for all guidance and support during the work, and for taking their time to answer questions outside the scheduled meetings. I must also thank the technical staff at EPT for all their help in the laboratory – the experiment would not be possible without it.

Finally, I would also like to thank Gisle Marhaug (NTNU Student services) for valuable motivational talks throughout my final year, which is much appreciated due to the absence from my studies for several years.

*Trondheim, 20 September 2019*

Henning H. Mathisen

## Abstract

The use of wood stoves has long traditions in Norway, both for heating and comfort. As modern houses are well insulated with small heat loss and wood stoves typically have large heat release, new solutions should be developed to level out this mismatch, to reduce the risk of overheating the room.

Latent heat storage (LHS) represents an interesting concept for temporary storage of thermal energy, especially with respect to the peak effects during batch combustion in wood stoves. This study entails such a concept, where the purpose was to experimentally test a compact, passive and durable LHS unit to be integrated on wood stoves. The concept is imagined placed on the stove top and consists of a coaxial stainless-steel container wrapped around the exhaust gas pipe, filled with high-density polyethylene (HDPE) which acts as a phase change material (PCM). The main advantage of using PCM to store heat, is the utilization of latent heat during melting, which is later released when the phase change is reversed. This results in higher energy density and lower weight for the unit compared to traditional solutions with sensible heat storage, e.g. soapstone. The aim was that the LHS unit should be able to store substantial part of the peak effects, leading to more stable heat release from the wood stove and thus improved thermal comfort.

The main challenge for the design was to facilitate for fast melting and slow solidification of the PCM for a realistic combustion duration, while keeping the max temperature below its thermal gradation point. This was important to avoid deterioration of the material, which will affect the thermal performance and durability of the LHS unit. Preliminary testing proved that oxidation posed a problem, which was counteracted by wetting the PCM with thermal oil.

The experimental design for the concept consisted of a 90-degree slice of the container and a heat cable inserted into a custom-made copper heating plate to simulate the stove top heat flow. Thermocouples were used to measure temperatures in different layers of the PCM and temperature control in the heating plate assured that degradation was avoided. The test rig was properly insulated to achieve a reasonable heat balance.

The primary test consisted of two different cycles; the first was completely insulated, whilst the side wall insulation was removed during the second cycle. The container was only half-full of PCM due to limited time for the primary test. Nevertheless, it can be viewed as a demonstration of the concept. The average temperature in the PCM at charge end was well above its melting point, ensuring latent heat storage. However, there were large temperature differences within the PCM, indicating absence of free convection. The PCM stored 0.4 kWh such that it would store about 3.2 kWh when scaled up to the final concept, assuming similar temperature development, which is about half of the desired heat to store. The effective thermal conductivity for the PCM was estimated and proved similar to literature values, supporting the assumption of only conduction heat transfer.

Due to the temperature control in the heating plate, the heat load decreased rapidly when setpoint was reached. This proved to be a weakness in the experimental design, as it was part of the goal to test the concept for a maximum heat flow. Heat transfer enhancement (HTE) can help to store more heat in the PCM and a brief fin analysis was done to propose a new container design, consisting of 8 internal radial fins, for future testing. Alternatively, metallic foam can be beneficial with respect to the LHS unit weight.

# Sammendrag

Bruken av vedovner har lange tradisjoner i Norge, både når det gjelder oppvarming og hygge. Moderne hus er gjerne godt isolerte med lite varmetap og siden vedovner typisk har høy varmeavgivelse, kan dette føre til overoppheting av rommet. Nye løsninger bør derfor utvikles for å redusere dette gapet.

Latent varmelagring (LHS) utgjør et interessant konsept for å lagre termisk energi, spesielt i forhold til vedovner som typisk har høy variasjon i varmeavgivelsen under forbrennings-forløpet. Denne studien omhandler et sånt konsept, der hensikten var å teste en kompakt, passiv og pålitelig varmelagringsenhet for vedovner. Konseptet er tenkt plassert på toppen av ovnen og består av en ringformet beholder i rustfritt stål som omkranser pipeløpet. Beholderen er fylt med «høy-tetthets polyetylen» (HDPE) som opptrer som et faseendringsmateriale (PCM), som gir fordel av å utnytte den latente varmen som absorberes under smelting og som senere blir avgitt når materialet størkner. Dermed kan store mengder varme lagres i forhold til lagerets volum, altså med større energitetthet, slik at varmelagringsenheten vekt blir lavere sammenlignet med tradisjonelle løsninger, som f.eks. ovner med kleberstein. Formålet med den latente varmelagringsenheten er å kunne lagre en betydelig del av ovnens varmeavgivelse, som fører til mer stabil varme til rommet og dermed bedre termisk komfort.

Den største utfordringen med designet var å muliggjøre rask smelting og sakte størkning for et realistisk forbrenningsforløp, og samtidig holde den maksimale temperaturen i PCM-en under degraderingspunktet. Dette er viktig for å unngå forringelse av materialet, som igjen vil påvirke den termiske yteevnen og påliteligheten til LHS-enheten. PCM-en ble fuktet med en termisk olje for å beskytte mot oksidering, som innledende tester påviste at kunne være et problem.

Eksperimentet bestod av en kvart beholder og en varmeplate i kobber der en varmekabel var montert for å etterligne varmeavgivelsen from toppen av vedovnen. Termofølere ble brukt for å måle temperaturer i ulike lag av PCM-en og varmeplata hadde temperaturkontroll slik at degradering ble unngått. Testriggen var også tilstrekkelig isolert for å oppnå en rimelig varmebalanse.

Hovedtesten bestod av to forskjellige sykluser hvor den første var totalt isolert, mens den andre var uten isolasjon på beholderens sidevegg. Beholder var bare halvfull med PCM på grunn av begrenset tid, men kan likevel anses som en god demonstrasjon av konseptet. Den latente varmen ble utnyttet, siden den gjennomsnittlige temperaturen in PCM-en var godt over smeltepunktet på slutten av varmebelastningen, men det var store temperaturforskjeller innad i materialet. Dette indikerte at det ikke forekom noe frikonveksjon. Den lagrede varmen i PCM-en var 0.4 kWh som vil tilsvare omtrent 3.2 kWh hvis man skalerer testen opp til det endelige konseptet, antatt en lignende utvikling for temperaturen. Dette utgjør ca. halvparten av den varmen som er ønskelig å lagre. Den termiske konduktiviteten til PCM-en ble estimert til å være nærme teoretiske verdier, som igjen støttet antagelsen om kun konduktiv varmeledning.

På grunn av temperaturkontrollen i varmeplata, ble varmebelastningen raskt redusert når settpunktet ble nådd, som igjen førte til at konseptet ikke ble testet for maksimum varmepåkjenning. Forbedring av varmeledningsevnen kan øke lagret varme i PCM-en og et forslag til et nytt design med 8 innvendige radielle finner er inkludert, for fremtidige tester. Alternativt kan andre metoder brukes, som metallisk skum.

## Table of contents

## Nomenclature

| | |
|---|---|
| $UA$ | Overall thermal transmittance (W/K) |
| $U$ | Thermal transmittance (W/m$^2$·K) |
| $L$ | Latent heat (kJ/kg) |
| $c_p$ | Specific heat capacity (J/kg·K) |
| $k$ | Thermal conductivity (W/m·K) |
| $T_m$ | Melting temperature (°C) |
| $T_G$ | Degradation temperature (°C) |
| $T_\infty$ | Ambient temperature (°C) |
| $C_r$ | Performance factor latent heat (-) |
| $C_{crit}$ | Performance factor risk of degradation (-) |
| $E_m$ | Young's modulus (GPa) |
| $q$ | Heat transfer rate (W) |
| $q'$ | Heat transfer rate per unit length (W/m) |
| $q''$ | Heat flux (W/m$^2$) |
| $Q$ | Total enthalpy (J) |
| $m$ | Mass (kg) |
| $A$ | Surface area (m$^2$) |
| $P$ | Perimeter (m) |
| $r$ | Radius (mm) |
| $Ø$ | Diameter (mm) |
| $\Delta T$ | Temperature difference (°C) |
| $\Delta x$ | Distance (m) |
| $\Delta z$ | Vertical distance between TC |
| $h$ | Heat transfer coefficient (W/m$^2$·K) |
| $Ra$ | Rayleigh number (-) |
| $g$ | Gravitational acceleration =9.81 m/s$^2$ |
| $L_c$ | Characteristic length (m) |
| $T_{film}$ | Film temperature (K) |
| $Nu$ | Nusselt number (-) |
| $Pr$ | Prandtl number (-) |
| $VF$ | Melted volume fraction (-) |
| $H_i$ | Respective height (m) |
| $H_T$ | Total height (m) |
| $R_i$ | Thermal resistance (m$^2$·K/W) |
| $L_f$ | Fin length (m) |
| $T_f$ | Fin tip temperature (°C) |
| $T_b$ | Fin base temperature (°C) |
| $m_f$ | Corrected convective fin tip (m$^{-1}$) |
| $A_c$ | Fin cross-sectional area (m$^2$) |
| $w$ | Fin width (m) |
| $t$ | Fin thickness (m) |
| $L_{cf}$ | Characteristic fin length (m) |
| $A_f$ | Fin surface area (m$^2$) |
| $U_f$ | Fin heat transfer value (W/m$^2$·K) |
| $R_f$ | Fin thermal resistance (m$^2$·K/W) |
| $C_f$ | Performance factor fin (W/kg) |
| $N$ | Number of fins (-) |
| $p$ | Pressure (mmHg) |
| $X_i$ | Measured value |
| $\Delta X_i$ | Individual uncertainty |
| $R$ | Calculated result |
| $\Delta R$ | Calculated uncertainty |
| $P$ | Heat cable power (W) |
| $V$ | Voltage (volt) |
| $I$ | Electric current (ampere) |

**Greek letters**

| | |
|---|---|
| $\alpha$ | Thermal diffusivity ($m^2/s$) |
| $\beta$ | Thermal expansion coefficient ($K^{-1}$) |
| $\varepsilon$ | Emissivity (-) |
| $\eta_f$ | Fin efficiency (-) |
| $\mu$ | Dynamic viscosity ($kg/m \cdot s$) |
| $\nu$ | Kinematic viscosity ($m^2/s$) |
| $\rho$ | Density ($kg/m^3$) |
| $\sigma$ | Stefan-Boltzmann constant $=5.67 \cdot 10^{-8}$ $W/m^2K^4$ |

**Subscripts**

| | |
|---|---|
| *solid* | Solid-state property |
| *liq* | Liquid-state property |
| *stored* | Stored in material |
| *cond* | Conductive |
| *conv* | Convective |
| *rad* | Radiative |
| *i* | Respective parameter |
| *table* | Towards table |
| *tray* | Insulation tray/box |
| *w* | Surface wall |
| *mean* | Average value |
| *max* | Maximum value |
| e*ff* | Effective |
| *cu* | Copper |
| *bot* | Bottom surface |
| *f* | Fin |

**Abbreviations**

| | |
|---|---|
| *LHS* | Latent heat storage |
| *PCM* | Phase change material |
| *HDPE* | High-density polyethylene |
| *HTE* | Heat transfer enhancement |
| *CNC* | Computer numerical control |
| *TC* | Thermocouple |
| *PI* | Proportional-integral (controller) |
| *MV* | Manipulated value |
| *PV* | Process value |
| *SP* | Set point |
| *CFD* | Computational fluid dynamics |
| *C1* | Insulated cycle |
| *C2* | Semi-insulated cycle |
| *HAZOP* | Hazard and operability study |

## List of Tables

## List of Figures

# 1 INTRODUCTION

## 1.1 Background

The use of wood stoves for heating and comfort has long traditions in Norway. In modern houses which are well insulated, this often creates a mismatch between heating need and supply, which then poses a challenge with respect to thermal comfort.

The energy use in Norwegian households was 47.6 TWh in 2017, which constituted 22 % of the total energy consumption that year [1]. Even tough electricity accounts for most of the household consumption, 5.8 TWh came from biofuels (mainly wood) which was the second most used source for heating [1]. Further, 25 % of the households have wood stoves as their primary heat source, where about 1.3 million metric tonnes of wood are incinerated each year [2]. Hence, wood is an important renewable energy resource.

Modern wood stoves with efficient combustion typically have a nominal effect of 8 kW, while the nominal heat loss for passive houses is 3 kW (Oslo climate) [3]. Hence, it is important to develop solutions with either lower effect or a thermal mass, to level out this mismatch and further reduce the risk of overheating the room.

Latent Heat Storage (LHS) represents an interesting concept of temporary thermal energy storage in many applications, especially when its desirable to store peak effects of heating or cooling. This makes the concept promising for wood stoves with batch combustion of wood logs, due to the transient heat production with high peak effects.

Phase Change Materials (PCM) are used to store the latent heat when the material undergoes phase change, usually from solid to liquid, with further heat release when the phase change is reversed. PCMs can typically store 5-14 times more heat than materials with only sensible heat storage [4], e.g. soapstone which is traditionally used for heat storage on wood stoves. Thus, high energy density and low weight can be achieved for the storage unit. Though many PCM materials are well documented in the literature, their implementation is still limited due to the complexity of designing suitable interfaces between PCM, heat source and heat sink. Further, to successfully commercialize a LHS unit for wood stoves, the aesthetic design is likely as important as the thermal performance, due to customer expectations [5].

A study by Sevault et al. [6] investigated a LHS concept for wood stoves, with erythritol in a container placed along the stove pipe. Numerical simulation of the concept was carried out, which proved that there was a challenge regarding the thermal degradation temperature for the selected PCM, which is only 42°C above its melting temperature. This posed a risk for deterioration of the material, which in turn would affect the durability of the unit.

The previous project work [7] dealt with a slightly different LHS concept, with a container filled with high-density polyethylene (HDPE), placed on top of the wood stove. The goal was to numerically model and analyse this compact, passive and durable LHS system which should be able to store a substantial part of the heat release during batch combustion and effectively releasing the stored heat to the room for several hours after the last batch. This would result in more stable heat release from the wood stove, ultimately improving the thermal comfort in the room.

## 1.2 Objective

The purpose of the Master thesis is to finalize the design of a LHS unit for wood stoves, which has been the focus of the previous Project work [7]. Build-up and implementation in the laboratory testing facility, as well as running the first experimental test campaign, are included in the plan.

The following plan was proposed to carry out the Master thesis:

1. Literature review focusing on:
    a. Practical issues linked to thermal energy storage using PCMs
    b. Experimental design and instrumentation of heat storage systems using PCMs
2. Experimental design
    a. Dimensioning of PCM unit according to available results from numerical studies
    b. Implementation of instrumentation equipment
    c. Calibration and preliminary tests of experimental setup
3. Experimental test campaign
    a. Determination of experimental test matrix to benchmark the setup
    b. Experimental tests according to test matrix
    c. Analysis of experimental results

## 1.3 Report structure

*This section is meant to give an overview of the report, by briefly explaining the content of each chapter:*

*Chapter 1* is an introduction with background on LHS and its application on wood stoves, problem description and objective of the master thesis.

*Chapter 2* contains a literature study on practical issues regarding phase change materials and experimental design of such storage units.

*Chapter 3* presents the concept, the selected PCM and the experimental design of the base case storage unit, which is to be tested experimentally.

*Chapter 4* contains the experimental results from both the preliminary tests and the primary test, which includes detailed analysis and discussion.

*Chapter 5* deals with analysis of heat transfer enhancement in the PCM, which forms the basis for a proposed container design including internal fins for future testing and comparison to the base case.

*Chapter 6* holds the conclusion and proposal for further work.

# 2 LITERATURE REVIEW

## 2.1 Practical issues for thermal energy storage using PCMs

When using phase change materials for thermal energy storage, there are several challenges which occurs. Hence, certain measures should be taken to avoid unwanted effects, primarily with respect to the material properties.

Thermal degradation is especially important to prevent, as it will change the material composition. The unique properties of polymers, such as HDPE, are a result of the polymer chain size. Degradation will break down the chain (polymer to monomer) and consequently reduce the material performance.

A study by Zauner et al. [8] found that HDPE was durable with respect to its thermophysical properties for more than 1000 thermal cycles of heating and cooling. To avoid oxidation, the test was performed under a nitrogen atmosphere, due to heat and oxygen at the same time is critical for HDPE, as proven in many chemical industries. The study also pointed out that PCMs for high-temperature applications should have high energy density and that its properties must be stable during the storage lifespan. In addition to have large phase change enthalpy, the difference in the melting and solidification range should be small.

Another study by Gasia et al. [9] investigating LHS systems under partial loads, focusing on three different parameters: health risk, thermal and cyclic stability. HDPE was one of several PCMs investigated (with latent heat, L=211-233 kJ/kg). It was found that HDPE is not hazardous under any conditions and the max temperature where it is thermally stable was found to be 309°C (slightly higher than theoretical value of 300°C). Note that in this study, it was assumed worst-case scenario with air in continuous contact with the PCM, risking significant oxidation.

Regarding the cyclic stability, the PCMs were tested for change in thermophysical and chemical properties during 100 cycles of phase changes (melting and solidification), using thermogravimetric analysis. The aim was to study the consequences of numerous cycles, with possible change in properties due to material degradation or thermal stress, which in turn will affect the LHS system durability and thermal performance. HDPE was found to have almost constant properties during 100 test cycles, although with small variations in its latent heat. This could be due to degradation of the chemical structure, with increasing number of cycles, leading to formation of some new compounds which have different latent heat compared to the fresh PCM. Further, some supercooling was occurring, resulting in somewhat lower phase change enthalpy during solidification.

Based on the three parameters, HDPE was evaluated to be suitable for LHS concepts with temperature range between 120 to 200°C, which is relevant to the application on wood stoves. It was non-hazardous, had no more than 12 % loss in thermal storage capacity after 100 cycles, and there were no significant changes in its chemical structure [9]. Also, it has low price as it is a common plastic which is produced in high volumes.

During the solidification process, a thermodynamic phenomenon known as supercooling can occur, which is the state where liquid solidifies below its normal melting point. In other words, the solidification temperature is somewhat lower than the melting temperature.

Supercooling can be understood as a delay in the solidification start during cooling of a material, where crystallization starts somewhat below the melting temperature. Hence, this effect leads to reduced crystallization temperature and thus the latent heat will be released at lower temperature. Consequently, a large temperature difference between charge and discharge is needed to utilize the latent heat [10].

Also, as the specific heat capacity changes with temperature, the degree of supercooling in the PCM will influence the solidification process, perhaps preventing the material from solidifying. This effect limits the application of PCM for thermal heat storage, notably for low-temperature applications, and can be handled by adding different agents to the material. Note that the effect of supercooling is more significant in inorganic PCMs (e.g. salt hydrates), whereas in HDPE (organic) the sub-cooling is less severe [11].

Further, regarding LHS application for wood stoves, there are several important criteria for the selection of PCM. It should have low thermal degradation, high values for both specific heat capacity and density, and a suitable melting temperature. Also, it should have low corrosivity, be non-toxic and inflammable [5].

## 2.2 Experimental design of heat storage systems using PCMs

In recent years, there has been an increasing focus on the use of PCMs for thermal energy storage. Different PCMs have been tested experimentally, although the selected PCM for the application on wood stoves has not yet been tested.

*This chapter is rather brief, as the experiment was designed from scratch. However, regarding the instrumentation, notably the thermocouples placement, some similar set-ups were found.*

In the study by Zauner et al. [8], which aimed to characterize HDPE as a PCM, experimental testing was carried out using an insulated steel container housing a fin-tube heat exchanger. It was filled with 170 kg HDPE pellets in total which melted slowly, with some deformation in the fins due to the thermal expansion. After several cycles of melting, crystallization and refilling of pellets, as the polymer shrunk in the crystallized state and leaving voids in the material, a yellowish colour appeared at the HDPE surfaces, most likely due to oxidation. In addition to flow meters, temperatures were logged in four different layers along the length of the storage.

In a study by Ytredal [12], the thermal conductivity of erythritol was investigated experimentally, both by heat supply from the top (only conduction) and bottom (convection included) of the storage unit, which was well insulated. The aim was to study the free convection effect on heat transfer and estimate the conductivity of the PCM. Due to the poor thermal conductivity of erythritol, the test set-up applied vertically placed thermocouples to measure temperatures throughout the material.

Further, it is well known that most PCMs suffer from low thermal conductivity and most studies involve some sort of Heat Transfer Enhancement (HTE) to promote the phase change process [13]. The most common type is radial fins due to their simple structure and low manufacturing cost. Metallic foam is another promising solution to increase the conductivity, posing a composite together with the PCM.

As the PCM is imagined encapsulated by a container, this will affect the heat transfer during phase change. During start of melting, both the stove and the container have significantly higher temperatures compared to the PCM. The bottom layer melts first, as the heat flow comes from below, and can act as an insulating layer due to the lower thermal conductivity at liquid state. This is likely to happen before free convection can set. During solidification, with heat transfer to the room, the PCM will solidify at the container walls first. This will then form an insulating layer, resulting in slower heat release, which can be beneficial regarding the aim of more stable heat release. On the other side, it can be too slow and pose a problem when the next combustion cycle is initiated, with the risk of overheating the PCM. This can be handled by adding HTE to the PCM, such as fins, metallic foam or heat pipes [5].

# 3 EXPERIMENTAL DESIGN

## 3.1 Concept and phase change material

The LHS concept is an annular container to be placed on top of the wood stove, wrapped around the exhaust gas pipe. It is assumed that 25 % of the stove's heat release is from the top, thus making it a proper placement for the LHS unit to store a substantial part of the peak effects.

As mentioned in Chapter 1, the typical heat release for modern wood stoves is 8 kW, such that 2 kW would pose the heat flow from the top. For a realistic combustion duration of 6 hours, this would amount to 12 kWh in total. The LHS concept should be able to store at least half of this heat.

Further, challenges regarding the unit design are to ensure melting and solidification of the PCM within reasonable time (stove operation), and at the same time storing enough heat to achieve stable heat release, while keeping the max temperature below degradation. An advantage of placing the unit on stove top, especially if module-based, is limited heat from pipe, thus not affecting the natural draught, which in turn is important to the combustion process.

The original design from project work [7] was slightly changed to achieve better heat transfer to room, as the container outside thermal resistance was a limiting factor, due to the poor heat transfer to air. This was done by increasing the diameter of the coaxial cylinder and reducing its height, such that the volume was unchanged, for comparison. However, this improved the outside UA-value by only 4 %. On the other hand, the changed geometry is more compact and may appear leaner, whereas the aesthetic design of the concept is important due to customer expectations [5]. The change in diameter also makes the heat flux from stove top to container bottom slightly smaller, as the heat flow is spread across a larger surface area.

Further, to test the concept experimentally, thermal expansion of the phase change material needed to be considered, whereas it was neglected in the numerical analysis in the project work. This was addressed by adding an increment to the top plate of the container, based on the potential maximum expansion in the PCM, where the change in its volume was used to find the angle of the increment. In the final concept, the expansion from the encapsulated PCM will likely lead to some pressure build-up in the container, which can be solved by including a valve. On the other hand, this might lead to air leakage into the container, risking repeatedly oxidation.

The new dimensions and 3D model of the concept are shown in fig. 3-1.

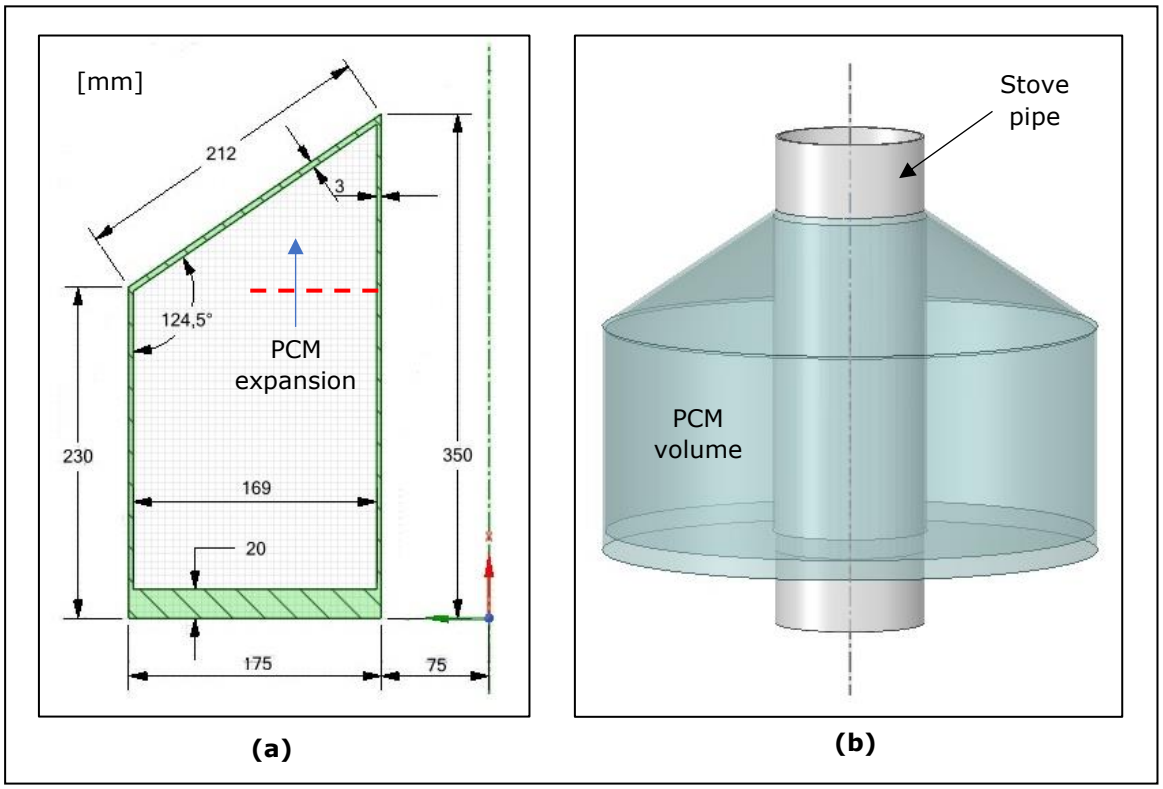


**Figure 3-1:** LHS concept; (a) PCM container dimensions; (b) 3D model including stove exhaust gas pipe

As for the project work, the selected PCM for the concept is HDPE, high-density polyethylene, a thermoplastic polymer produced from ethylene. This is a highly available and relatively cheap material, as it is used for many every-day products, e.g. plastic bottles. Its properties [14] are listed in Table 3.1. Note that the density, specific heat and thermal conductivity are a function of temperature, thus values for both solid and liquid state are listed (see Appendix A for more details). The HPDE ordered for the experiment was in the form of shavings.

For normal operation of wood stoves, the typical wall temperature is about 160°C during the peak effects [15]. This makes HDPE suitable for a LHS system applied on wood stoves, as its melting temperature is lower than the stove's wall temperature, ensuring phase change and utilization of the latent heat. Further, it should be able to withstand higher temperatures in case of burst firing by stove operator. The relatively high thermal degradation temperature of HDPE is promising with respect to avoiding deterioration of the material.

Note that the solidification temperature range in Table 3.1 is somewhat lower than the melting temperature. This is due to the supercooling effect, as mentioned in Chapter 2.1. This effect is most significant in applications with small temperature range, where the latent heat may not be rejected, whereas for a wood stove with large temperature difference to room temp, this is not an issue.

**Table 3.1** – HDPE material properties

| **Properties** | | **Value** | **Unit** |
|---|---|---|---|
| Density, $\rho$ | *solid (25°C)*<br>*liquid (150°C)* | 960.0<br>801.6 | $kg \cdot m^{-3}$ |
| Specific heat, $c_p$ | *solid average*<br>*liquid average* | 2200<br>2700 | $J \cdot (kg \cdot K)^{-1}$ |
| Thermal conductivity, $k$ | *solid (25°C)*<br>*liquid (150°C)* | 0.55<br>0.21 | $W \cdot (m \cdot K)^{-1}$ |
| Dynamic viscosity, $\mu$ | | 0.001 | $kg \cdot (m \cdot s)^{-1}$ |
| Latent heat of fusion, $L$ | | 245 | $kJ \cdot kg^{-1}$ |
| Melting temperature range | | 129 - 134 | °C |
| Solidification temperature range | | 125 - 122 | °C |
| Thermal degradation temperature, $T_G$ | | 300 | °C |

Further, in addition to the appropriate melting temperature of HDPE, to perform well as a LHS system, a performance indicator $C_r$ as described by Kristjansson et.al. [16] is given by *eq. (3.1)*. The ratio compares the latent heat relative to the sensible and latent heat. In other words, the portion of latent heat stored in the pcm compared to the total heat needed for melting.

$$C_r = \frac{L}{c_{p,solid}(T_m - T_\infty) + L} \qquad (3.1)$$

Where $L$ is the latent heat, $c_{p,solid}$ is the specific heat in solid state, $T_m$ is the melting temperature and $T_\infty$ is the ambient temperature. If $C_r$ is low, then the heat storage is like that of a sensible heat storage, e.g. soapstone. The ratio is important for applications where the melting temperature is far from the ambient temperature, as in this case.

Regarding potential thermal degradation, another ratio [16] is the overheating indicator $C_{crit}$, given in eq. *(3.2)*, which expresses the extra heat needed to reach degradation temperature after melting is complete. This gap should be large, hence $C_{crit}>1$.

$$C_{crit} = \frac{c_{p,solid}(T_m - T_\infty) + L + c_{p,liq}(T_G - T_m)}{c_{p,solid}(T_m - T_\infty) + L} \qquad (3.2)$$

When evaluating these indicators for HDPE, as listed in Table 3.2, with an assumed room temperature ($T_\infty$) of 20°C, it performs well whereas half of the heat stored is latent and that it needs almost twice the amount of heat to reach degradation. Thus, HDPE is a suitable PCM for the LHS concept.

**Table 3.2** – HDPE performance indicators

| | $C_r$ | $C_{crit}$ |
|---|---|---|
| HDPE | 0.49 | 1.90 |

Another practical issue regarding PCMs, as mentioned in section 2.1, is the potential oxidation of the material when in air contact, which will reduce the thermal performance of the pcm. Since the pcm shavings must be filled into the container in advance, thermal oil was used to protect HDPE from air, as a measure to avoid oxidation. The selected oil was Duratherm 630, a heat transfer fluid with similar properties as HDPE, as it has hydrocarbon-based composition. The key factor considered, was that its density should be lower than that of HDPE, for the entire temperature range of the experiment, as shown in fig. 3-2. Thus, hopefully it would form a protecting layer between the denser pcm and the much less dense air.

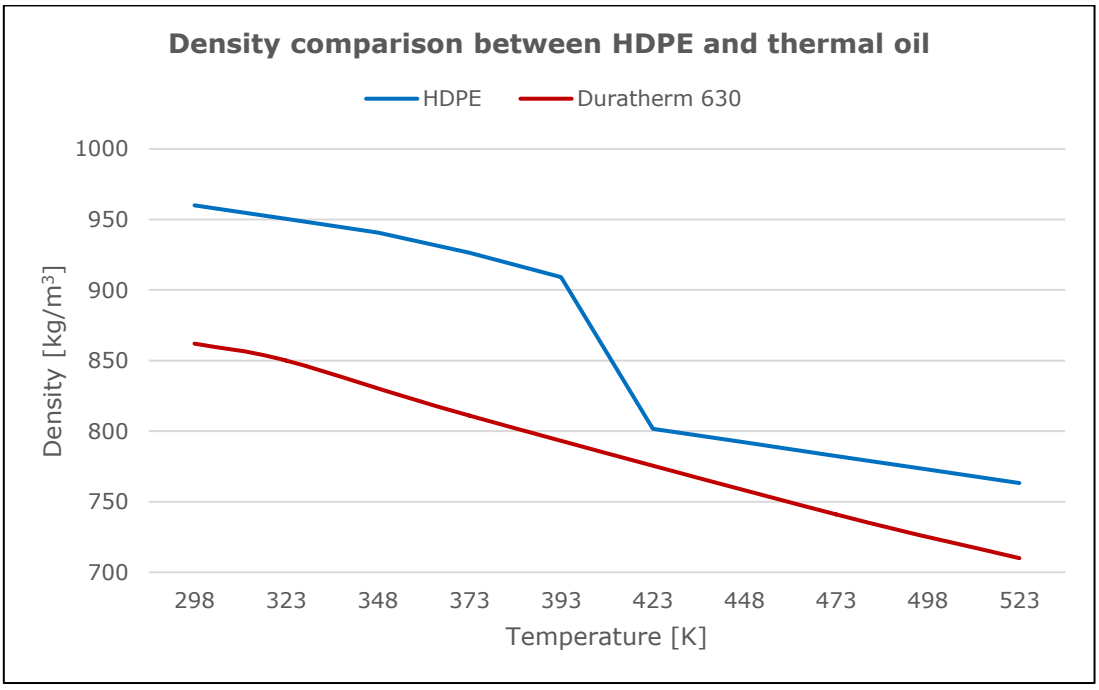


**Figure 3-2:** Density comparison between HDPE and thermal oil

As fig. 3-2 shows, the thermal oil's density is lower for the relevant temperature range, so it was considered a decent measure to prevent oxidation. Further, Duratherm 630 is ranked low on chemical reactiveness, nor is it toxic or hazardous to the environment, although

inhalation of vapor should be avoided. However, it has a flash point of 229°C and a fire point of 245°C [17], so one should be cautious with ignition sources. This was not an issue for the experiment. The oil's auto-ignition temperature is 367°C, well above the operating temperature for the test.

## 3.2 Test rig container for PCM

For the original concept, the container material was aluminum due to its good thermal properties, notably the thermal conductivity. However, for the experimental test, it was decided that the container should be built in stainless steel, as it was desirable to test the concept for a maximum heat flux to investigate risk of thermal degradation in the pcm. For temperatures close to 300°C ($T_G$), it was a concern that an aluminum container would experience buckling, as the Young's modulus, $E_m$, decreases with increasing temperature. The container was designed with an opening at the top to avoid pressure build-up, hence buckling would probably not be an issue. Nevertheless, stainless steel was selected for container material as a safety measure, as it has better stiffness compared to aluminum, as listed in Table 3.3 along with other material properties [18] of interest.

The steel used in the container is 316 austenitic type. Due to the much lower thermal conductivity of steel, it was regarded as a good demonstration of the concept. Regardless, HDPE has significantly lower value for $k$.

**Table 3.3** – Properties of stainless steel (316) and aluminium

| **Property** | **Steel** | **Alu** | **Unit** |
|---|---|---|---|
| Density, $\rho$ | 7800 | 2700 | kg/m$^3$ |
| Specific heat, $c_p$ | 500 | 910 | J/(kg·K) |
| Thermal conductivity, $k$ | 15 | 237 | W/(m·K) |
| Emissivity, $\varepsilon$ | 0.9 | - | - |
| Young's modulus, $E_m$ (at 260°C) | 180 | 60 | GPa |

Since the concept is axisymmetric, it was further assumed that a 90-degree slice of the container would be sufficient to demonstrate the concept's thermal performance, as a similar temperature development was expected along its cross-sectional area. On the other hand, to angle should not be to small, as heat loss from side section walls would affect the heat flow in the pcm.

Further, a quarter of the concept required a quarter of the heat flow from the stove top, hence 500 W to test for maximum heat flux (the flux is the same). During the design of the container and when considering how the heat load should be applied to it, as discussed in chapter 3.3 below, a heat cable was planned to supply the heat. However, it was difficult

to find a suitable cable that would supply 500 W in such a small area, hence the container height was reduced by half to get less pcm to heat. This was based on the initial heat cable selected, which could supply approx. the half of the desired heat load.

Due to the reduced container height, the increment angle seen in fig. 2-1 could be decreased, as the smaller amount of pcm would pose less thermal expansion. Also, as the material from the original concept was changed to stainless steel, the thickness of both the bottom plate and side walls was reduced, due to the far larger density of steel (as seen in Table 3.3). This change was necessary regarding production considerations for the curved plates and with respect to container weight. The steel plates were cut using water jet and then assembled by welding. Note that the density for 316 steel is closer to 8000 kg/m$^3$, but the listed value is used for the calculations.

Figure 3-3 shows the dimensions of the test rig container and how it appears in 3D, where the z-axis represents the centerline of the exhaust gas pipe. This design is further referred to as the base case design, whereas there is no heat transfer enhancement (HTE), e.g. fins or metallic foam. The initial goal was to build several containers with different design, as proposed in the project work [7], for comparison. However, the build-up in the lab and preparation (pcm filling and melting of pcm shavings) for the primary test needed far more time than expected, so this experiment must be regarded only as a demonstration of the concept.

In hindsight, based on the project work results [7], fins should have been implemented for HTE in the pcm, but due to the simplified numerical model and the changes (both geometry, material and heat flux) for the test rig container, it seemed important to test the base case as a starting point. This will also serve as reference frame for future testing.

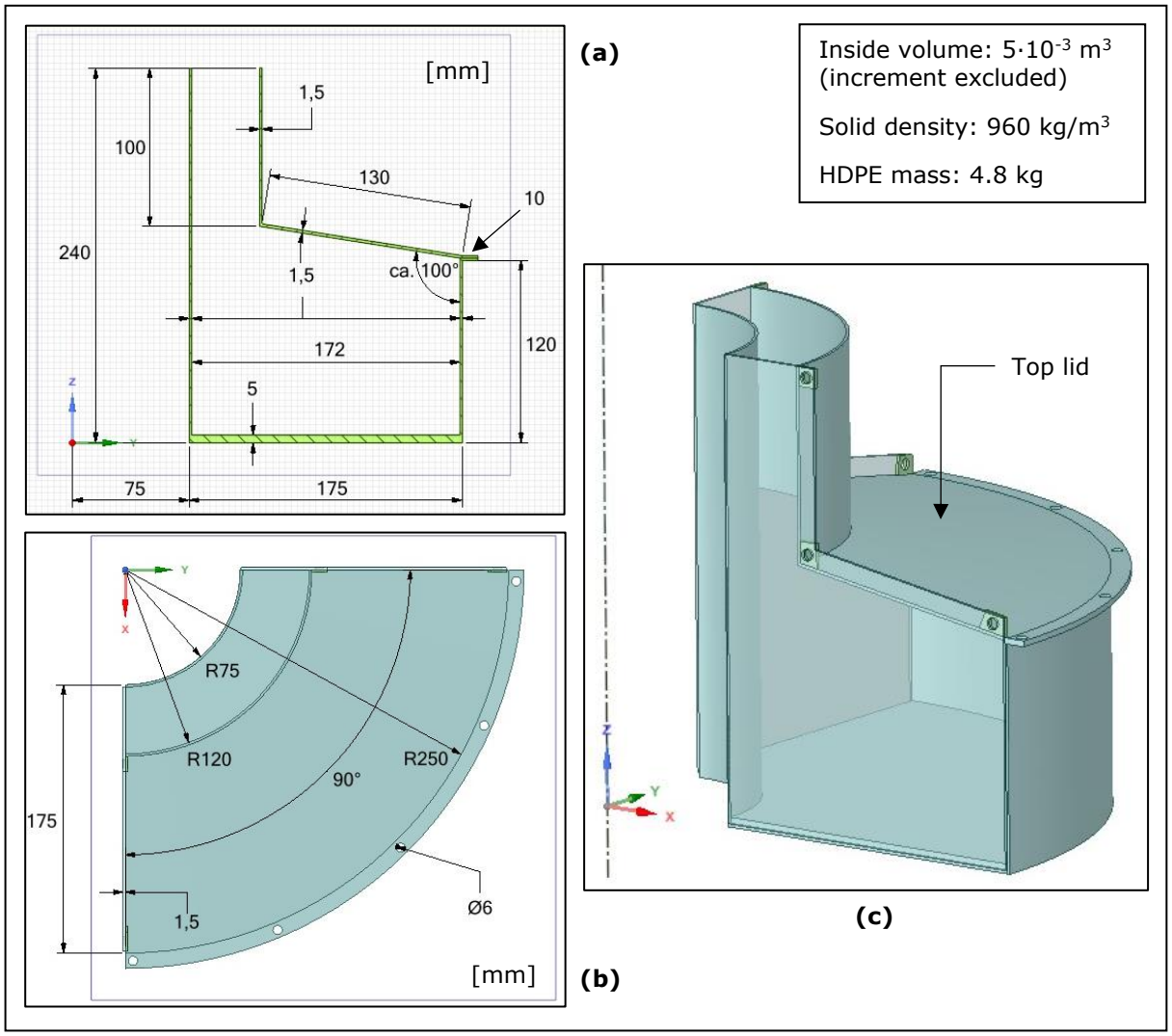


**Figure 3-3:** Test rig container; (a) cross-sectional dimensions; (b) radial dimensions viewed from top; (c) 3D model

It was first imagined that the container would have a top lid, as displayed in fig. 3-3, such that filling of pcm (and later removal) would be easier. Since the flanges was welded on to the container, it resulted in some buckling which proved difficult to compensate with sealings. It was important to keep the lid tight onto the container to avoid leakage during the expansion of the pcm, so it was decided that the entire lid was welded. The purpose of the top opening, initially to avoid pressure build-up and to leave room for expansion of the pcm and thermal oil, then served for pcm filling as well. The finished container is seen in fig. 3-4, although the pictures were taken before the lid was welded tight.

**Figure 3-4:** Finished container with cannula pipes

## 3.3 Heating plate

To simulate the heat flux from wood stove top, a heating plate was needed below the pcm container. The aim was to get an evenly distributed heat flow to the container bottom, as it would experience if integrated on a wood stove. Hence, the heating plate was designed with the same radial dimensions as shown in fig. 3-3-b, such that its surface area would match that of the container bottom. Copper was selected for the plate's material, due to its superior thermal conductivity, such that it would be able to supply a uniform heat flow, as mentioned. The properties of copper [18] are listed in Table 3.4.

Further, it was essential for both the heating plate and the container bottom plate to be as plane as possible, to achieve good surface contact between the two, avoiding extra thermal resistance. Both components were produced to specification, although the container had some buckling from the welding process, which was attempted to correct by manual grinding, with little success. Alternatively, copper paste could be added enhance the heat transfer, but would probably float away during heating. However, this gap was very small, so this was disregarded as a problem.

Buckling was also considered for the heating plate, as this component would experience the largest temperature differences and consequently the most thermal stress. The heating plate was produced by an external supplier, using a CNC machine to mill a track for the heat cable, such that heat load would be distributed evenly from the inside. Due the good thermal conductivity of copper, the plate will be uniformly heated, so will the thermal expansion, hence no significant strain across the plate should occur. If any, it should be negligible compared to the yield strength.

**Table 3.4** – Properties of copper

| **Property** | **Value** | **Unit** |
|---|---|---|
| Density, $\rho$ | 9000 | kg/m$^3$ |
| Specific heat, $c_p$ | 350 | J/(kg·K) |
| Thermal conductivity, $k$ | 410 | W/(m·K) |
| Young's modulus, $E_m$ (at 260°C) | 100 | GPa |

Regarding the heat cable, it was later found a more suitable cable (Isopad H900) to achieve the desired heat load. The initial one, which where the reason for the reduced container height, as mentioned in section 3.2, was able to provide 150 W per meter of cable length, whilst the selected one could supply 350 W/m. As the milled track length was approx. 1.5m, a total heat load of 525 W could be delivered. However, the H900 1.5 m cable supplies 540 W, based on supplier specifications [19]. The reason for change of heat cable was a misunderstanding between the cable's operating temperature versus its max withstand temperature. Figure 3-5 shows the 3D model of the heating plate, whilst the finished version with mounted heat cable is seen in fig. 3-6.

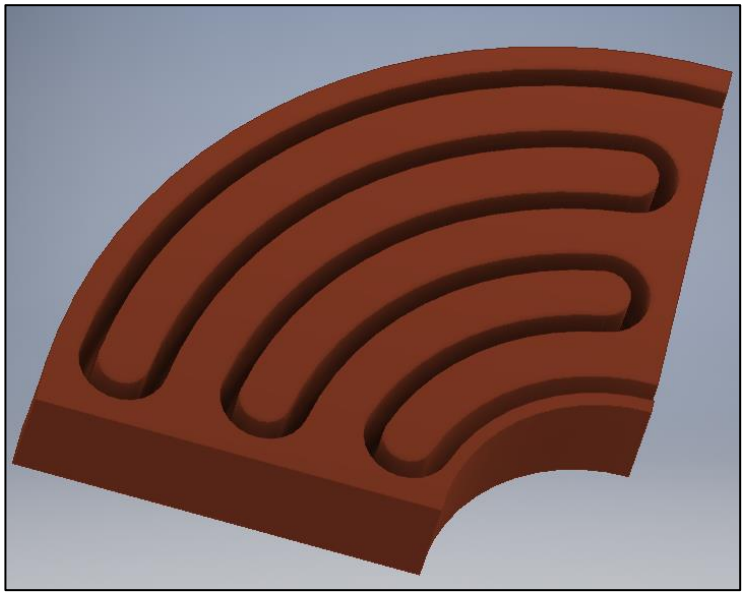


**Figure 3-5:** 3D model of heating plate with milled track for heat cable [20]

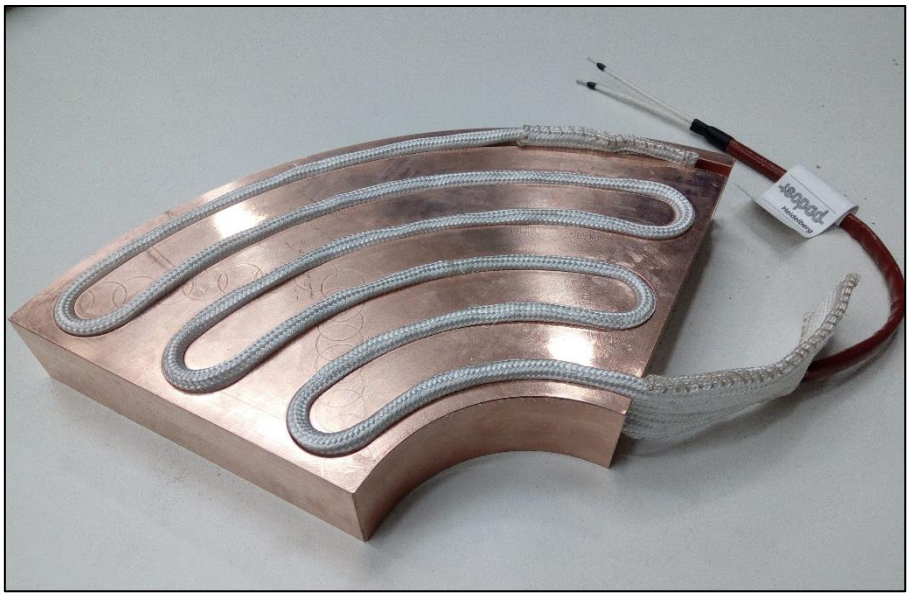

**Figure 3-6:** Finished heating plate with inserted heat cable

Since the heating plate is produced separately, it makes it possible to test other container designs with heat transfer enhancement or different PCMs, with the same set-up, as the container can easily be replaced.

## 3.4 Insulation and heat balance equations

The test rig needed to be insulated in order to limit the heat loss, as the concept's only real heat loss to room would be from the top and outer side wall of the container. Thus, the side section walls (90-degree slice) and pipe area was insulated. Note that some heat flow from the hot exhaust gas in the pipe should be expected, but if the concept is considered as a module-based product which can be easily installed on any wood stove, there would be a small air gap to the pipe, hence with a thermal resistance, so the heat flow from the pipe was disregarded in the test.

Further, there was build an insulation tray for the heating plate and container to be placed on, both as a practical measure to avoid burning the working table and to ensure as little as possible heat flow to the table. The heating plate represents the wood stove top, so this is where the heat supply is coming from, in other words, there should be no heat flow downwards (stove is hotter). The tray was built from one plate of Skamolex, an insulating board used inside wood stoves, two pieces of foam plates found in the lab of unknown material (possibly Silcapor) and it was covered with Fyrewrap LTF insulation (with aluminum foil to reduce radiation). The insulation properties are listed in Table 3.5, with the assumption that the foam plates have similar properties as Silcapor. The finished insulation tray is shown in fig. 3-7.

**Table 3.5** – Properties of insulation materials

| **Property** | **Skamolex** | **Foam plate** | **Fyrewrap** | **Unit** |
|---|---|---|---|---|
| Density, $\rho$ | 750 | 250 | 128 | kg/m$^3$ |
| Specific heat, $c_p$ | 950 | 800 | 700 | J/(kg·K) |
| Thermal conductivity, $k$ | 0.3 | 0.022 | 0.032 | W/(m·K) |
| Emissivity, $\varepsilon$ | - | - | 0.04 | - |
| Volume | 0.0025 | 0.01 | 0.03 | m$^3$ |
| Estimated mass | 1.875 | 2.5 | 3.84 | kg |

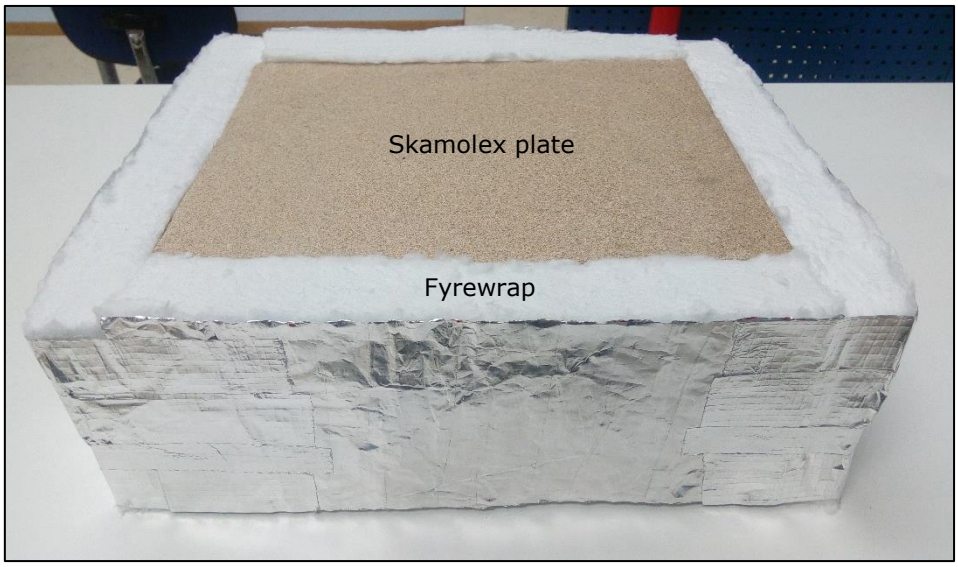


**Figure 3-7:** Finished insulation tray

The formulas used to estimate the test rig heat balance, are the equation for heat storage *(3.3)* and the basic equations for heat transfer; Fourier's law of conduction *(3.4)*, Newton's law of cooling *(3.5)* and Stefan-Boltzmann law of radiation *(3.6)*:

$$Q_{stored} = m_i c_{p,i}(T_i - T_\infty) \tag{3.3}$$

$$q_{cond} = \frac{kA\Delta T}{\Delta x} = U_{table} A_{tray}(T_i - T_\infty) \tag{3.4}$$

$$q_{conv} = h_i A_i (T_i - T_\infty) \tag{3.5}$$

$$q_{rad} = \varepsilon_i \sigma A_i (T_i^4 - T_\infty^4) \tag{3.6}$$

Where $Q_{stored}$ represents the stored heat, $q_{cond}$, $q_{conv}$ and $q_{rad}$ are the heat transfer rates by conduction, convection and radiation, respectively. The indicator *i* points out the measured values for each respective surface. Further, *m* is the mass, $c_p$ is the specific heat, *k* is the thermal conductivity, *A* is the surface area, $\varepsilon$ is the material emissivity, $\sigma$ is the Stefan-Boltzmann constant and $T_\infty$ is the ambient temperature. Note that conduction heat transfer is only considered for heat loss from the heating plate to the table, whereas $U_{table}$ is the effective heat transfer value for the insulation tray, based on the series of thermal resistances for the difference materials.

Further, the heat transfer coefficient $h_i$, which indicates the heat transfer rate between a surface and its surroundings (air in this case) for a given temperature difference, was estimated by the following procedure.

The heat loss to air is assumed to be caused by natural convection in the laminar regime, as the temperature differences are expected to be small. The Rayleigh number, *Ra*, is calculated, which is associated with buoyancy-driven flows and is given by eq. *(3.7)*, where the transition from laminar to turbulent flow occurs at $Ra=10^9$.

$$Ra = \frac{g\beta(T_{w,i} - T_\infty)L_c^3}{\nu\alpha} \qquad (3.7)$$

Where *g* is the gravitational constant, $\beta$ is the thermal expansion coefficient, $T_{w,i}$ is the respective surface wall temperature, $T_\infty$ is the ambient temperature, $L_C$ is the characteristic length, *v* is the kinematic viscosity and $\alpha$ is the thermal diffusivity.

The properties of air [21] are evaluated at film temperature $T_{film}$, which is the average temperature between the surface wall and ambient, which have been assumed to be 40°C. Although the film temperature will be different for each surface, especially for the test cycle where the container side wall insulation is removed (discussed later), the air properties are assumed to be constant for simplicity. Also, air is assumed to be an ideal gas such that $\beta=1/T_{film}(K)$.

Regarding the characteristic length; for the side walls, $L_c$ is the height of the respective wall. For the top wall, $L_c$ is given by eq. (3.10) where *A* is the surface area and *P* is the perimeter, which is equivalent to the sum of inner and outer circumference of the top wall, which is annular.

Further, the Nusselt number, *Nu*, is calculated based on empirical correlations for external free convection flows, as for vertical plates according to Churchill and Chu, and for horizontal plates [22]. The correlations are given by equations (3.8) and (3.9) respectively. The calculation of the heat transfer coefficients is shown in Table 3.6.

Correlation for vertical plates:

$$Nu = \frac{h_i L_c}{k} = 0.68 + \frac{0.67Ra^{1/4}}{[1 + \left(\frac{0.492}{Pr}\right)^{9/16}]^{4/9}}, \quad Ra \leq 10^9 \qquad (3.8)$$

Correlation for horizontal plates:

$$Nu = \frac{hL_c}{k} = 0.54\, Ra^{1/4}, \quad Ra\ \epsilon\ [10^4, 10^7] \tag{3.9}$$

$$L_c = \frac{A}{P} \tag{3.10}$$

**Table 3.6** – Air properties and calculation of heat transfer coefficients

| Air: $v=19\cdot10^{-6}$ m²/s; $\alpha=27\cdot10^{-6}$ m²/s; $\beta=3\cdot10^{-3}$ K⁻¹; $k=0.03$ W/(m·K) | | | | | |
|---|---|---|---|---|---|
| | **Side (outer)** | **Side (section)** | **Tray** | **Top** | **Unit** |
| *A* | 0.07 | 0.13 | 0.3 | 0.06 | $m^2$ |
| *P* | - | - | - | 0.66 | m |
| $L_c$ | 0.12 | 0.2 | 0.15 | 0.09 | m |
| $T_w$-$T_\infty$ | 20 | 30 | 10 | 20 | K |
| *Ra* | $2.03\cdot10^6$ | $15.1\cdot10^6$ | $2.13\cdot10^6$ | $0.92\cdot10^6$ | - |
| *Nu* | 20.1 | 32.7 | 20.3 | 16.7 | - |
| *h* | 5 | 4.9 | 4.1 | 5.6 | W/(m²·K) |

As Table 3.6 show, the heat transfer coefficients are small, hence the convective heat loss to air is limited. However, when the insulation is removed for the outer side wall of the container, the temperature difference increases significantly, and radiation also becomes an important factor. Consequently, h will also change, as it is a function of the wall temperature, but this was found to be only a small increase. This is discussed in more detail in Chapter 4.3.3 (heat balance). Note that the pipe area is included in the "side section" calculation. Also, *Ra* for all the surfaces are in magnitude of $10^6$ which indicates laminar flow, as expected.

*Note that h is calculated based on the experimental data for the temperature differences but is listed in this chapter to separate its method from the results.*

## 3.5 Instrumentation and control system

As the experiment is a study of heat transfer in PCM, temperature seemed as the key parameter to measure. Due to the poor thermal conductivity of HDPE, it was expected large temperature differences throughout the material, at least during start of discharge. Since the container is heated from the bottom, it was intuitive to measure temperatures in a vertical manner, as discussed in Chapter 2.2.

One option was to place the thermocouples (TC) at the top lid pointing downwards, with difference length into pcm mass. This way, they could easily be removed when filling the pcm or making other changes. However, this was abandoned as the top lid was welded tight. Another problem might that the thermocouples would be stuck in the solid pcm, as logging during discharge also was of interest. In addition, the vertical temperature gradient was expected to be large, so this may influence the measurement due to some conduction in the thermocouple.

Instead, the TC were placed along the side walls, both from pipe and outer wall, such that each TC series would have the same radial position, as seen in fig. 3-8. Both series were placed 45° relative to the side section walls, to avoid influence from heat loss at these walls. This would also make it easier to compare with future designs, e.g. with fins inside the container. Further, cannula pipes were soldered onto the container side walls, which made the insertion of the TC easy. The pipes holding T1-T5, which are placed at the center of the pcm mass, were supported by a steel bracket to ensure a stable position for the measurement points. This was important due to movement within the pcm, e.g. free convection or forces during phase change. T6-T10 were placed closer to the outer side wall to investigate the influence of heat loss in this region of the pcm.

Fifteen TC were acquired, 10 to be placed inside the container, one for temperature control in the heating plate and the remaining four to measure outside temperatures. For measurement of heat loss to room, heat flux sensors were also considered, but were found to be too expensive. Note that during the primary test, T5 and T10 was used to measure outside temperatures, for the side section wall and for a lid that was mounted on the container top opening, respectively. This was done due to the container only being half-full of pcm and is discussed further in Chapter 4.

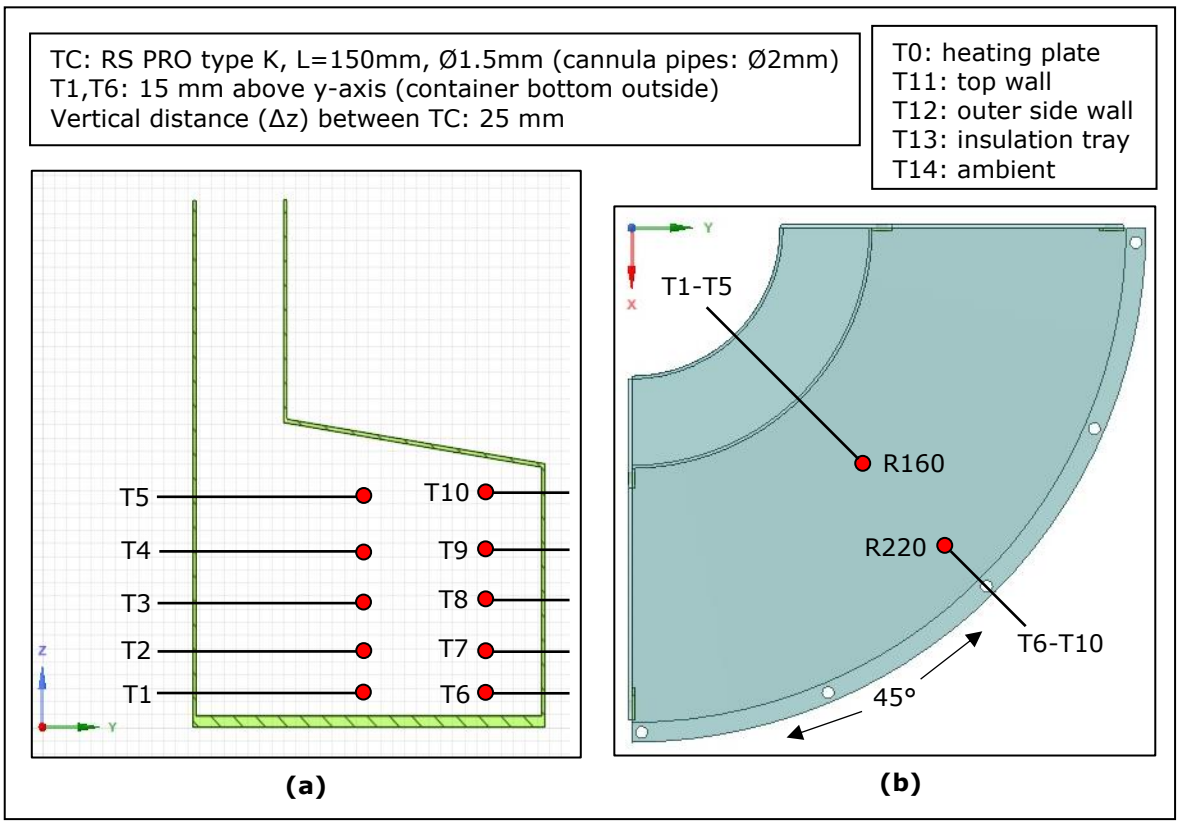


**Figure 3-8:** Thermocouples placement in container; (a) side view; (b) top view

The thermocouples were planned for calibration, but the laboratory calibrator was sent away for calibration itself, so an alternative method was used. It was attempted to calibrate the TC using ice water and boiling water as reference points. However, this simplified method was found to be too uncertain, with the risk of making the TC less accurate than the listed value of TC type K (± 2.2°C). See Appendix B for more details regarding the calibration attempt. Uncertainty analysis can be found in Appendix C.

Further, the temperatures were logged for each minute of flow time. The thermocouples and the heat cable were connected to a utility cabinet, with assorted electrical components, which then was connected to a computer with the software LabVIEW installed. This posed the control system for the experiment, which is shown by the sketch in fig. 3-9.

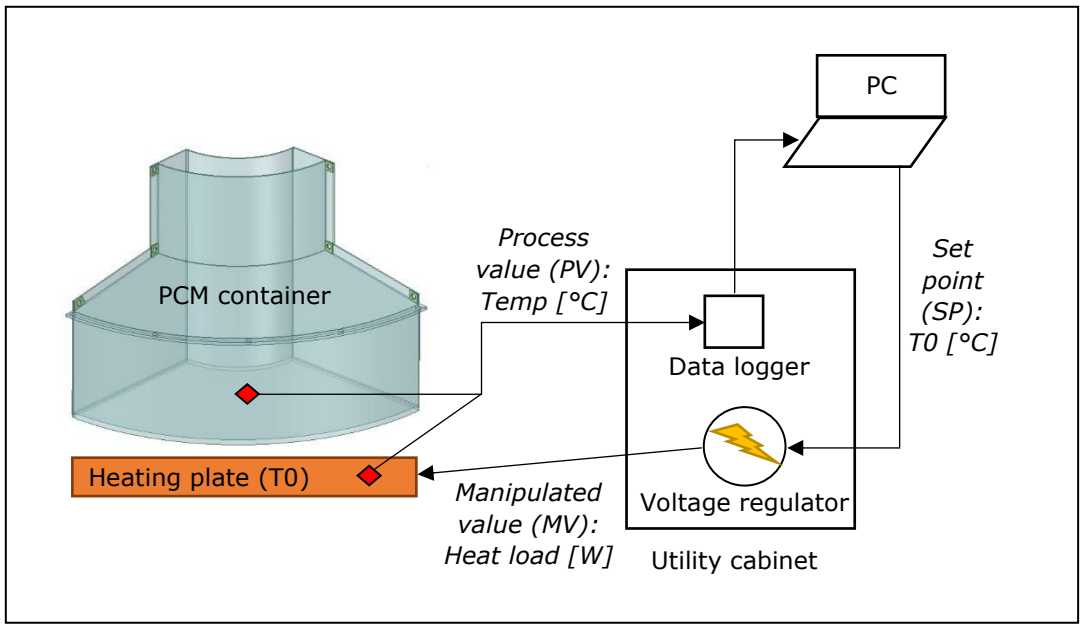


**Figure 3-9:** Basic sketch of experimental set-up with emphasis on the control loop

The heating plate temperature (T0) was selected as the control temperature for the system, to avoid the pcm from reaching degradation temperature. The set point for T0 was then adjusted to the desired temperature in the heating plate, whilst a PI-regulator was used to control the voltage regulator response, which then manipulated the heat load from the heat cable. When T0 reaches its set point, the heat load decreases accordingly. The tuning of the PI-regulator was first attempted according to the Ziegler-Nichols method [23] [24], with little success, and was rather tuned by testing the response in the current system.

Ventilation was also installed above the test rig, as some evaporation from both HDPE and thermal oil was expected. A picture of the set-up is seen in fig. 3-10. The risk assessment for the experiment can be found in Appendix D.

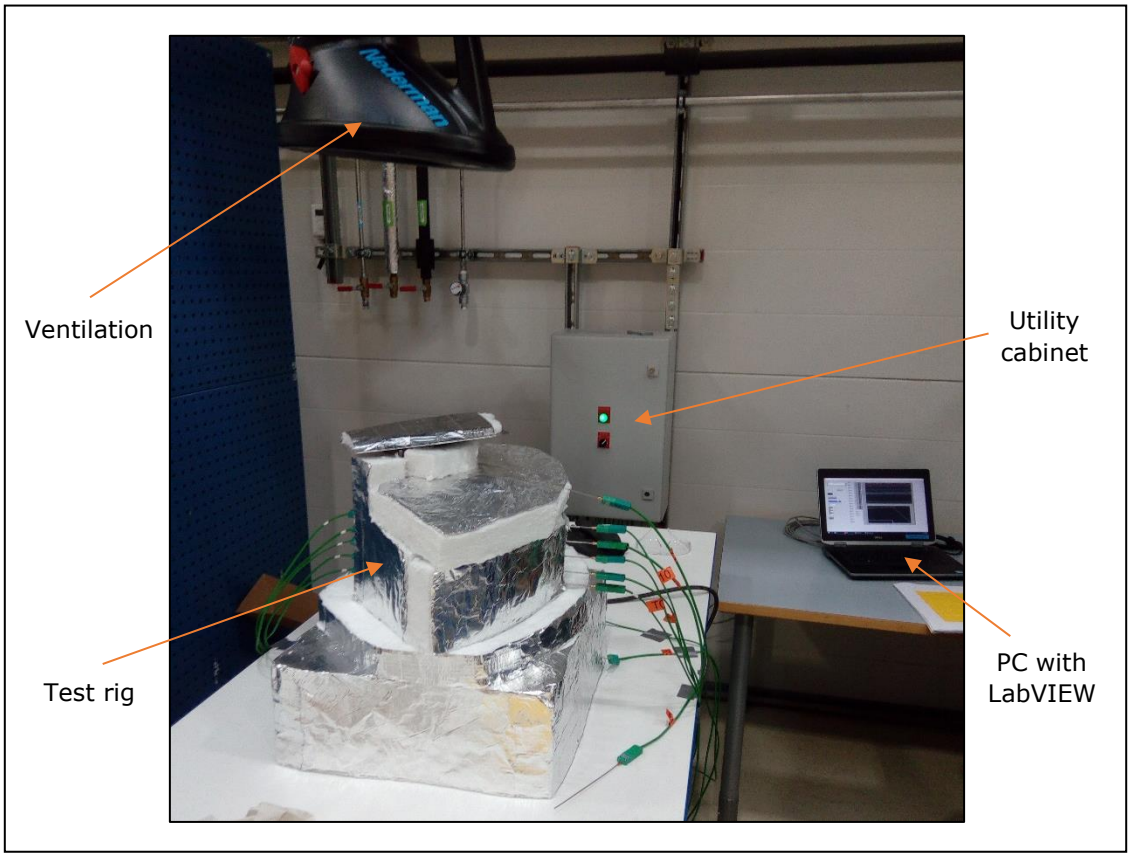


**Figure 3-10:** Picture of experimental set-up

## 3.6 Experimental test campaign

Several stages of preliminary testing were planned to prepare the test rig for a primary test. This included investigation of the compatibility between HDPE and the selected thermal oil (to prevent oxidation), container filling of the HDPE shavings and further melting the shavings into a solid mass. In addition, the PI-regulator tuning was important to control the heat load to avoid large overshoot in the heating plate temperature, potentially risking PCM degradation.

Table 3.7 shows an overview of the main test phases carried out, whilst the results are discussed in detail in chapter 4. The preliminary testing consists of test phase 1-2, whilst phase 3-4 are the preparation for phase 5, which is the primary test. Note that Table 3.7 is an updated version of the initial plan, due to various changes during the test campaign, as with any experiment.

**Table 3.7** – Experimental test matrix

| **Experimental test campaign** | | |
|---|---|---|
| **Test phase** | **Agenda** | **Method** |
| **1** | What: Compatibility test between HDPE and Duratherm 630<br>Why: To investigate porosity and density difference – Avoid air contact to prevent HDPE oxidation | Melted in frying pan |
| **2** | What: Several cycles of melting and solidification of HDPE with small amount of thermal oil<br>Why: To study the effect of potential oxidation and danger for degradation; changes in HDPE properties, notably melting temperature and colour | Melted in frying pan |
| **3** | What: Several stages of filling and melting of HDPE shavings in the test rig container, with low effect from heating plate (to avoid overheating)<br>Why: To get desired amount of HDPE (approx. 4.8 kg) | Low heating plate temperature |
| **4** | What: Complete melting of all HDPE shavings into a solid mass<br>Why: Remove air pocket between the shavings, as this affects both porosity, density and heat transfer within the PCM | Lid added to reduce heat loss from top opening |
| **5** | What: Run experiment for realistic charge and discharge; for two different cycles; insulated (C1) and semi-insulated (C2)<br>Why: For comparison and as a demonstration of the concept | Charge for realistic combustion duration |

Further, a numerical model was set up using the CFD software ANSYS Fluent 19.1, according to the same methodology used in the project work [7]. The goal was to predict the experiment outcome, for comparison and validation of the data. However, the numerical simulation was carried out during the experimental build-up. Unfortunately, the simulation was done with a constant heat flux at the container bottom, opposed to the constant temperature which was the case for the test. Thus, the simulation was invalid for comparison to the experimental data and is not included in this report.

# 4 RESULTS AND DISCUSSION

## 4.1 Preliminary testing

To investigate the compatibility of HDPE and Duratherm 630, various tests were carried out using a cooking plate and a frying pan to heat the mixture, as it was interesting to study the porosity, density difference, potential oxidation and further degradation at higher temperatures. In addition, it was of interest to find out whether any chemical reactions would occur, whereas both substances are based on hydrocarbons.

Further, a small amount of HDPE shavings was placed in the frying pan, as seen in figure 4-1, whilst a heat load was applied from the cooking plate. Temperature in HDPE was measured using a thermocouple strapped to the frying pan handler, such that the measuring point was surrounded by the HDPE shavings and at the same time avoiding contact with the frying pan bottom.


**Figure 4-1:** Preliminary test set-up; (a) frying pan with HDPE shavings; (b) thermocouple placement

Note that the uncertainties of the preliminary testing are disregarded, as the key interest was to investigate the HDPE behaviour during melting. Although, it should be mentioned that this simple set-up has poor temperature control in the pcm, as the heat load is regulated by power (vs temperature for the test rig). Neither is there probably uniform temperature in the pcm and impurities in the material may also affect the outcome.

Further, the TC placement in the frying pan can also change throughout the process, either with air contact or it may touch the pan. However, the evaluation is based on the measured temperature and visible changes.

### 4.1.1 HDPE melted without thermal oil

To study how HDPE itself behaves during heating, a small amount of the material (less than shown in fig 4-1) was put in the frying pan and temperature was logged during two cycles of charge and discharge. The results are shown in figure 4-2 below.

The intention of running a second cycle was to check if there were any changes in the PCM, although only a limited understanding can be achieved due to the simplicity of the test, e.g. change in material properties that are not visible. However, melting temperature and changes in colour were of interest, as it indicates oxidation.

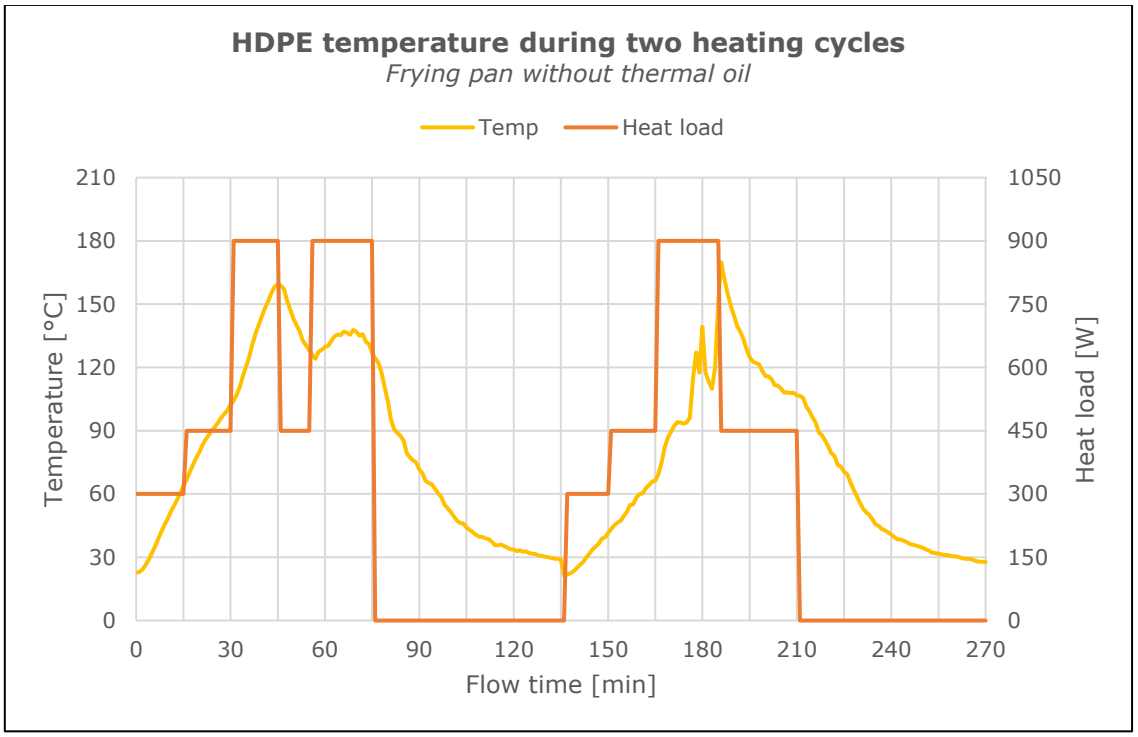


**Figure 4-2:** Temperature in HDPE without thermal oil during two heating cycles

During the first cycle, the heat load was reduced at 45 min due to much smoke development. Although far from degradation temperature, this could be the case due to the poor temperature control. Significant colour change was also visible. The instability at 180 min during the second cycle was caused by adjustment of the TC placement, as it had moved on top of the pcm mass. The pcm had solidified with some strain after the first cycle, such that an insulating layer of air between the pan and pcm was present, hence the heating during second cycle was slower.

Further, it's difficult to comment any changes in properties or melting temperature, as the pcm was in a rubbery state during melting, due to much heat loss (no lid on pan). However, at least it was found that air contact should be prevented, as both visible smoke and significant colour change indicates deterioration of the pcm. This is displayed in fig. 4-3, notably the brown discolouration which appeared.


**Figure 4-3:** Colour change in HDPE without thermal oil; (a) at melting temperature; (b) solidified at room temperature

### 4.1.2 HDPE melted with thermal oil

To study the effect of using thermal oil, two different test cycles were carried out; first with too much oil (soaked) and then with less oil, where the pcm were only wetted.

Note that the first cycle (fig. 4-4) was the carried out before the test with no oil but is included in this chapter for discussion of the oil. Also, it was done before the control system was ready, so the temperature was logged using a hand-held thermometer (type RS 1314).

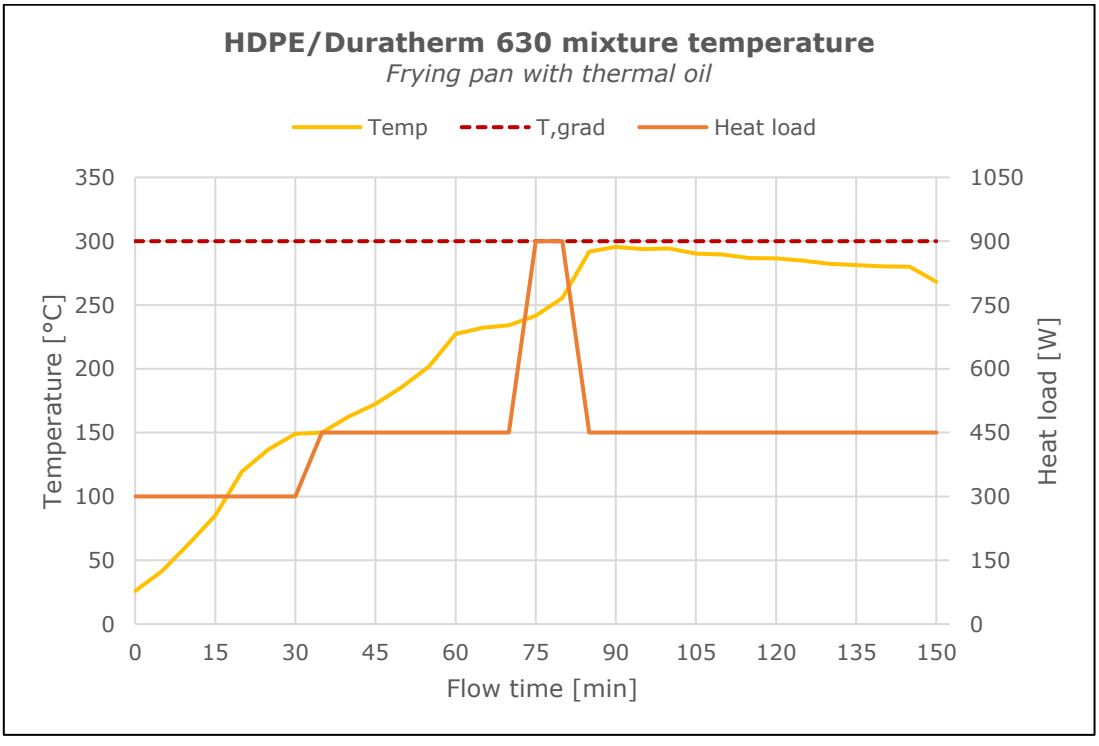


**Figure 4-4:** Temperature in HDPE soaked with thermal oil during one heating cycle

As seen from fig. 4-4, temperature was only logged during charge. Since the HDPE was soaked in thermal oil, a mixture formed during heating, opposed to the desired effect where the substances would separate, with the oil floating on top due to its lower density, posing a protecting layer against the air. The oil has similar properties compared to HDPE, both with respect to density, specific heat and thermal conductivity, hence with low thermal diffusivity. In addition, the void between the shavings were filled with oil, so this possibly why the mixture behaved as one substance. Further, the shavings on top did not melt due to significant heat loss to air (no lid).

After 90 min flow time, when the mixture reached 300°C, smoke appeared, indicating degradation. This could also be due to deterioration of Teflon in the pan, which occurs around 260°C. The results from this test also proved difficult to analyse due to the mixture formation, but at least degradation temperature was confirmed by the smoke and that the amount of thermal oil should be far less. Important to avoid this in primary test.

Further, a new batch of HDPE with much less thermal oil was tested, to find out if only wetting the shavings would protect it from air and prevent oxidation. A similar heat load pattern was applied, and discharge was also logged as shown in fig. 4-5. The temperature stabilized after 60 min when the pcm was in a rubbery state, so the heat load was increased to check if the temperature would stay constant or increase. Consequently, the temperature also increased, indicating that the HDPE was at steady state rather than the typical phase change curve. This was probably due to the large heat loss to air.

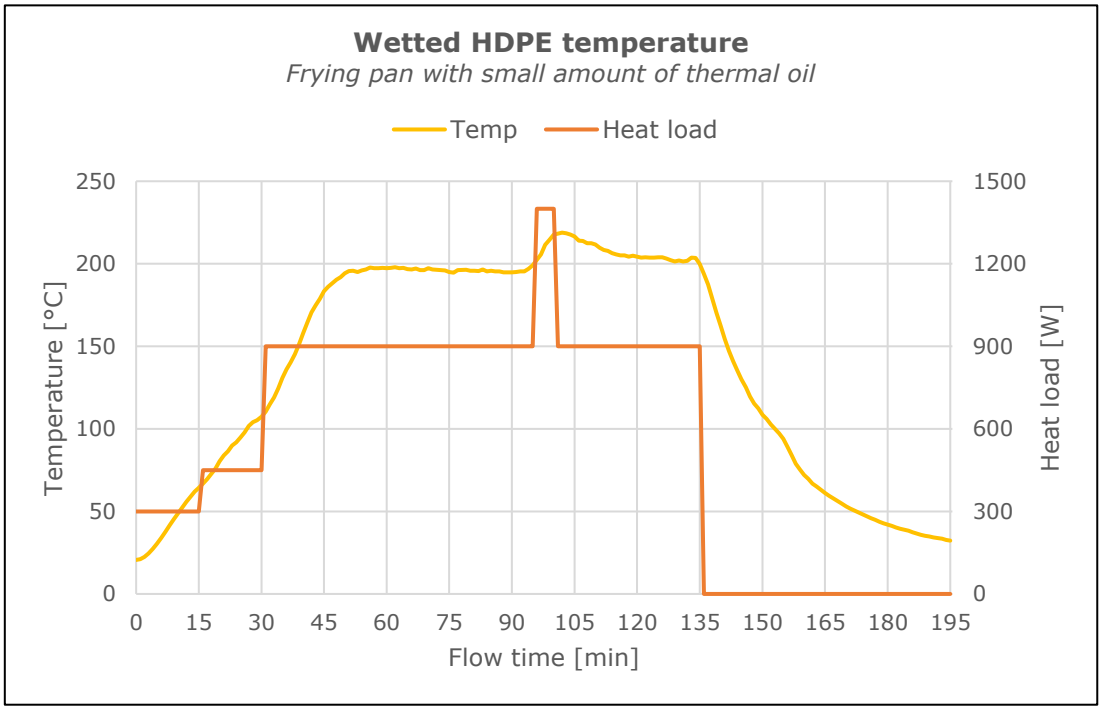


**Figure 4-5:** Temperature in HDPE wetted with thermal oil during one heating cycle

Further, there was some smoke visible after the heat load was increased to 900 W, although less smoke compared to the test with no oil. The colour was still clear and transparent during melting, which indicates that the oil prevents oxidation. However, when reaching 200°C, a brown colour along the circumference of the mass appeared. Also, there

was more smoke, perhaps caused by evaporation of the oil. Apart from this, it seemed as wetting the shavings was the best solution to avoid oxidation.

### 4.1.3 Summary of discussion

Three different tests were carried out to determine whether contact between HDPE and air would pose a problem during the primary test. Due to the simple method, where the pcm was melted in a frying pan, the evaluation was mainly based on visible changes.

The test where only HDPE was heated showed significant smoke development and colour change, indicating oxidation of the material. Different amounts of thermal oil were used to prevent this effect, both by soaking the shavings and by wetting them. The first resulted in a mixture between the substances, which would not be relevant for the concept with respect to utilizing the latent heat, due to only sensible heating of the oil. The second test, with wetted shavings, seemed as the most promising solution, whereas the colour was still clear during melting.

The initial goal for using a thermal oil, where it was imagined floating on top of the pcm due to its lower density, was not the case. The difference in density should probably be larger to get this effect, but it was difficult to find a suitable fluid because the boiling point would be a problem. Hence, based on the preceding tests, it was decided to use Duratherm 630 to prevent oxidation during the primary test, by wetting the shavings. Alternatively, inert gas could be used to displace the oxygen inside the container.

## 4.2 Container filling

Due to the HDPE was in form of shavings, the container had to be filled with batches which were melted together to a solid mass, before adding more shavings. To avoid overheating of the shavings at the container bottom, due to the material's low conductivity, 100 ml of thermal oil was added first. Each batch were weighed and then wetted with oil before it was placed in the container. The temperature in the heating plate (T0) was set far from degradation temperature, to further ensure slow melting of the shavings. The container was also fully insulated, to reduce the heat loss.

This process proved to be time consuming, as each batch had to melt to make room for the next one. Consequently, the filling had to be done in several stages, where the pcm mass had to be heated up from the previous day. Due to limited time, the container was only half-full before moving on to the primary test. Figure 4-6 shows the last filling stage carried out, with 2.1 kg HDPE and 300 ml (0.25 kg) thermal oil in total.

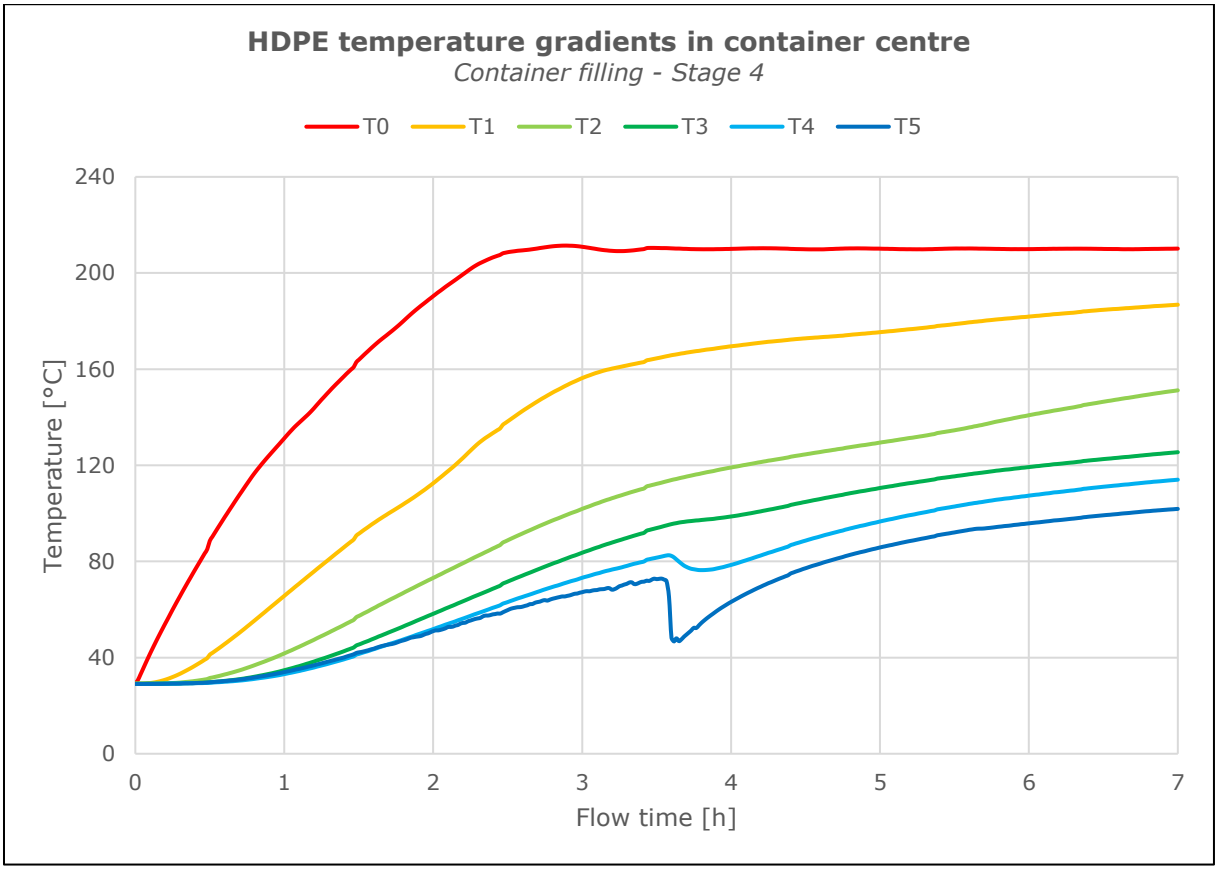


**Figure 4-6:** HDPE temperature gradients during last filling stage

The heat load during filling was approx. 50 % of the heat cable power until T0 reached its setpoint of 210°C, before decreasing to keep T0 stable. As the pcm got hotter, the heat load decreased further, as the temperature difference was smaller. The heat load was kept low to ensure gentle rise in heating plate temperature, thus with slow melting of the pcm. This could probably be done faster, but as it was during the break-in phase of the system, it was done more carefully.

Further, the filling of the last batch is clearly displayed by the temperature drop for T4 and T5 in figure 4-6, where the upper layer of shavings already in the container was mixed with shavings at room temperature. Note that these temperatures really show a pcm-air temperature, due to the void between the shavings. Also, with more pcm added to the container, the mass to be heated obviously increased. Hence, with larger thermal resistance and longer time to melt the shavings on top. After 7 hours flow time, there was a temperature difference of almost 90°C between T1 and T5, an indication of the low thermal conductivity of the material and air pockets.

At charge end (7 hours), the upper layers of HDPE were not melted, although T3 had just reached the melting point. The layers below are assumed melted together, most notably for T2 which has a slight increase in its temperature gradient at 5.5 hours, indicating that melting is complete. Also, T2=134°C at this point, which is the melting temperature of HDPE. The same pattern is not as visible for T1, but the slightly steeper gradient just after 2 hours may indicate that this layer has melted, due to the lower conductivity at liquid state, hence the faster increase in temperature (heat transfer to layers above is slower).

Before the primary test could be initiated, it was important that all the shavings were melted to a solid lump, as it would be for the final concept. In other words, the heat transfer would be through the pcm without any air pockets. To help the melting process, a lid was placed on the top opening, heating plate temperature was increased to 230°C and charge duration was increased to 8 hours. The temperature development is seen in fig. 4-7.

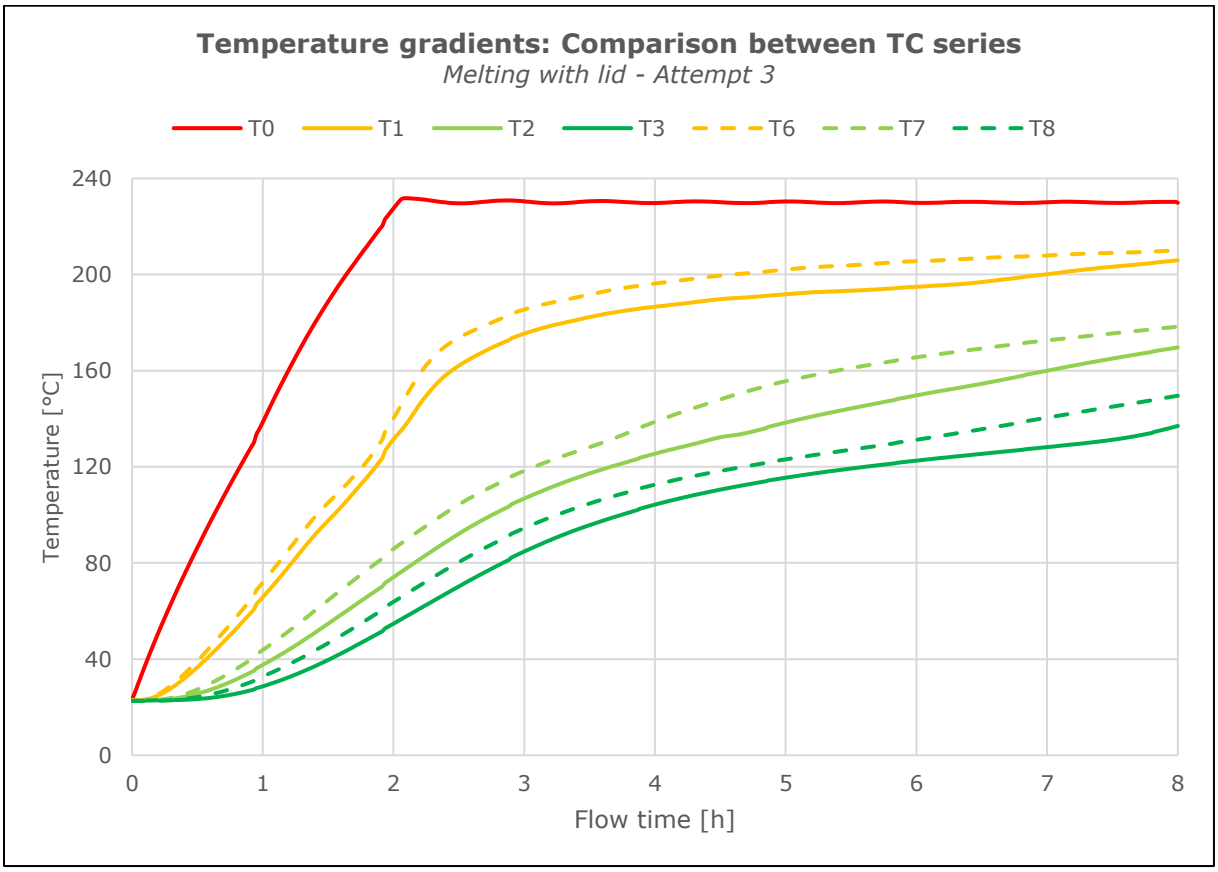


**Figure 4-7:** Temperature development during melting process of HDPE shavings

Note that T4 and T5 are excluded from fig. 4-7, as the pcm mass had shrunk down when being melted together, whilst these thermocouples then measured air temperature in the container. These were later used to measure outside temperatures to estimate heat loss.

Further, there was carried out several attempts to melt all the pcm (still some shavings on top), hence the "attempt 3" notation in fig. 4-7. The TC series at outer wall is also included, where the same colour indicates the same vertical level in the container (same layer). As seen, T6-T8 are consistently higher compared to T1-T3, most likely due to heating from container side wall and possibly influenced by conduction in the cannula pipes.

The temperature development is similar to that of the filling stage, although the heat load was slightly higher during the melting attempt, as seen by the steeper gradient for T0, consequently reaching its setpoint faster. Comparing the temperature difference between T1 and T3 at 7 hours flow time, which was 60°C during filling and 70°C during melting, might be due to a larger total temperature difference for the latter, with higher T0 and T3 closer to air in the container. In addition, this large temperature difference within the pcm suggests that there is no free convection, whereas the difference in temperature should decrease due to the convective effect (mixing of layers). Hence, the HDPE is not entirely liquid, rather in a viscous rubbery state. This further advocates for the use of heat transfer enhancement (HTE) in the pcm, e.g. fins or metallic foam.

However, melting is complete at charge end with T3=137°C, which is above the melting point. As seen in fig. 4-7, the gradient for T3 also becomes steeper at charge end, indicating that phase change is over. Further, it should be mentioned that T3 continues to increase during start of discharge, due to heat flow from the layers below. This is addressed for the primary test in next chapter. Also note that the gradient for T1 gets steeper at 6.5 hours flow time, presumably due to less heat loss to the above layers which gets hotter.

A visual check proved that all the shavings were melted, as shown in fig. 4-8, although this picture was taken after solidification. Note that the solid pcm has contracted away from the side walls, leaving a small air gap which poses a thermal resistance.

**Figure 4-8:** HDPE shavings melted into a solid lump

## 4.3 Primary test

To study the thermal performance of the LHS concept, two different test cycles were run. The first cycle (C1) were completely insulated, whilst the insulation on the outer side wall of the container was removed during the second cycle (C2), as seen in fig. 4-9. Apart from this, both cycles were run for the same charge time (6 hours) and with the same setpoint for heating plate temperature (275°C). This was assumed to be a realistic combustion duration for regular operation of wood stoves, while keeping the max temperature safely below the thermal degradation point of HDPE. Temperatures were also logged during discharge (18 hours) to study the development for 24-hours until next charge the following day.

Although the HDPE mass in the container was only half of the designed amount (desired mass to demonstrate the concept), this test can be viewed as an indication of the concept's potential.

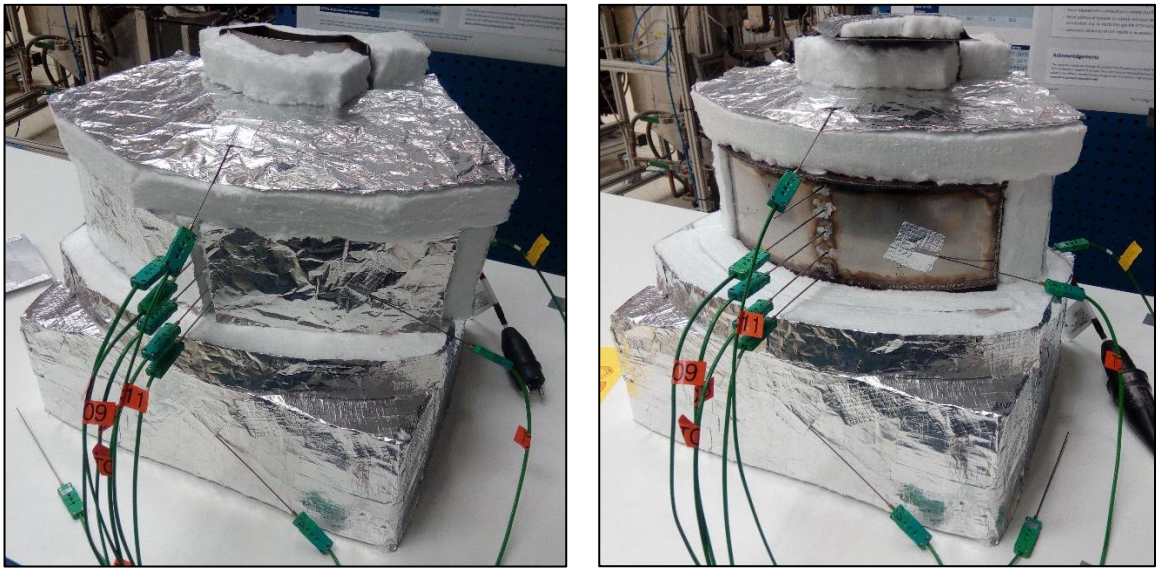

Insulated (C1) Semi-insulated (C2)

**Figure 4-9:** Difference in set-up between the two primary test cycles

### 4.3.1 Temperature development

Since the container was only half-full, the average temperature in the PCM, $T_{mean}$, was calculated for thermocouples T1-T3 and T6-T8. There was a small difference in initial temperature in both the PCM and the heating plate, where it was about 8°C higher for C1 due to a heating cycle from the previous day. This difference was assumed to be negligible with respect to the comparison between the two cycles, as the temperature range was much larger.

Regarding the heat load, it was applied max power (100 %) until T0 reached 270 °C, then the PI-controller was tuned such that the power decreased rapidly to about 50 % and further with auto-regulation for a setpoint of 275 °C. This method was done similar for both cycles, and the purpose was to avoid too much overshoot in the heating plate temperature.

To figure out how much power that was needed to maintain a stable temperature in the heating plate, the temperature gradient (dT/dt), e.g. the slope of T0 in fig. 4-10, was calculated at about 1 hour flow time and compared to the theoretical gradient if the entire heat load went to heating the heating plate (no heat loss). The difference was found to be approx. 50 %, thus half of the heat load was heating the heating plate and needed to be reduced accordingly to stabilize T0.

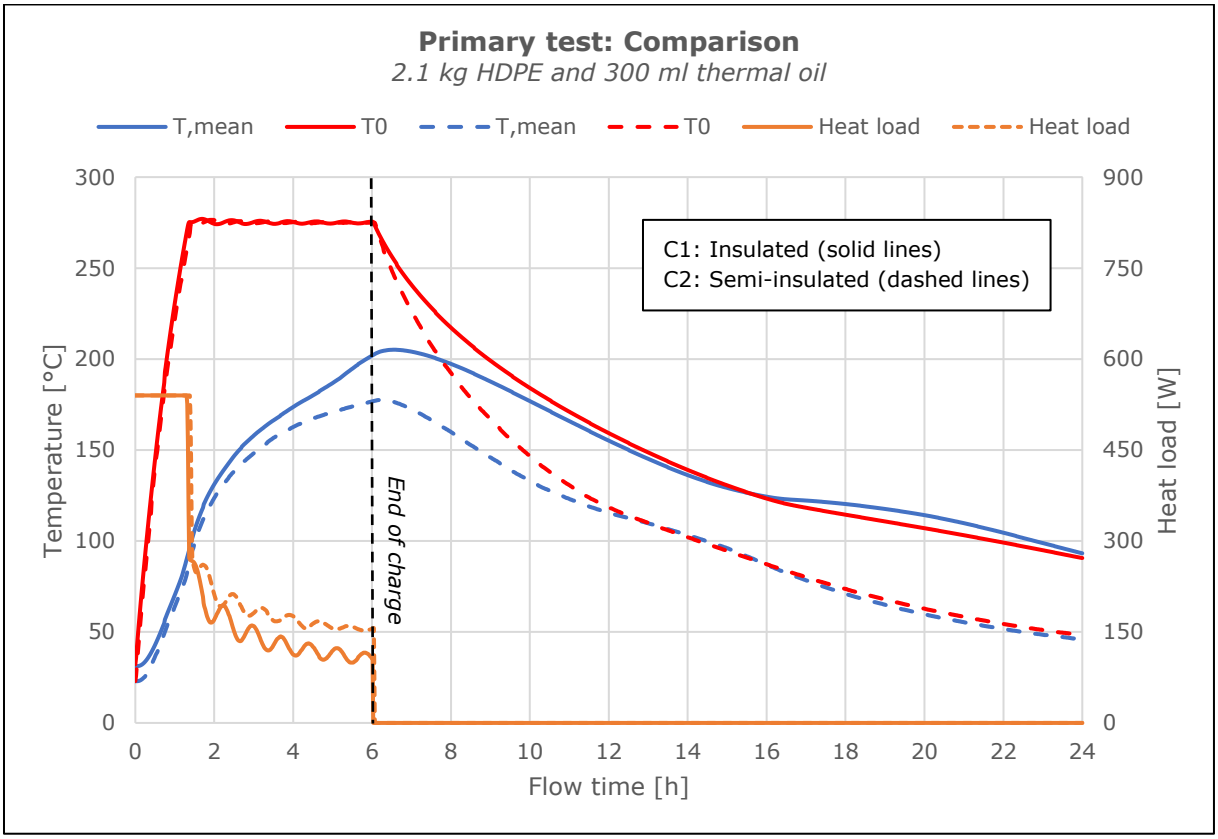


**Figure 4-10:** Primary test comparison; Temperature development vs heat load

As displayed in fig. 4-10, note that when the pcm temperature increases, the temperature difference between T0 and $T_{mean}$ decreases, thus the heat loss from the heating plate to pcm gets smaller. Consequently, less power is needed to sustain the setpoint for T0, hence the heat load decreases as well. Also, the heat load (MV) fluctuates more than T0 (PV) due to the large thermal mass of the heating plate. In other words, the change in T0 is slow compared to the change in power (could also be affected by the PI-controller tuning).

Further, its seen that the heat load is slightly larger while the average temperature is somewhat smaller during C2. This is due to the removal of the outer side wall insulation which makes the heat loss larger. Hence, the pcm heats more slowly while more power is

required to keep T0 at its setpoint. This is also displayed during discharge, where T0 decreases more rapidly during C2.

Initially, the goal was to test the LHS concept for a realistic combustion duration with max heat load (as an imitation of burst firing), but this was limited due to the design of the experiment. Instead of a constant heat load of 500 W to the container, significant parts of the applied heat load were stored in heating plate (large thermal mass). Due to the temperature control, the heat load decreased towards charge end, e.g. to approx. 150 W during C2. Thus, the heat load was only 30 % of the desired value.

Although the heating plate is not a part of the LHS concept, the gentle increase its temperature is considered a good imitation of the wall temperature on a wood stove.

Further, as the removal of the side wall insulation was the only modification done between the two cycles, the TC series placed at this wall (T6-T8) showed a significant difference. Compared to the centre TC series (T1-T3), it was measured higher values for C1 and lower for C2, as expected due to change in heat loss. However, the placement of T6-T8 may have been too close to the container wall, leading to the measurements being affected by conduction through the cannula pipes. Even though T6-T8 were included in the average temperature in fig. 4-10, a better comparison between the two cycles was assumed to be for T1-T3, which are placed at the container centre. This comparison is seen in fig. 4-11.

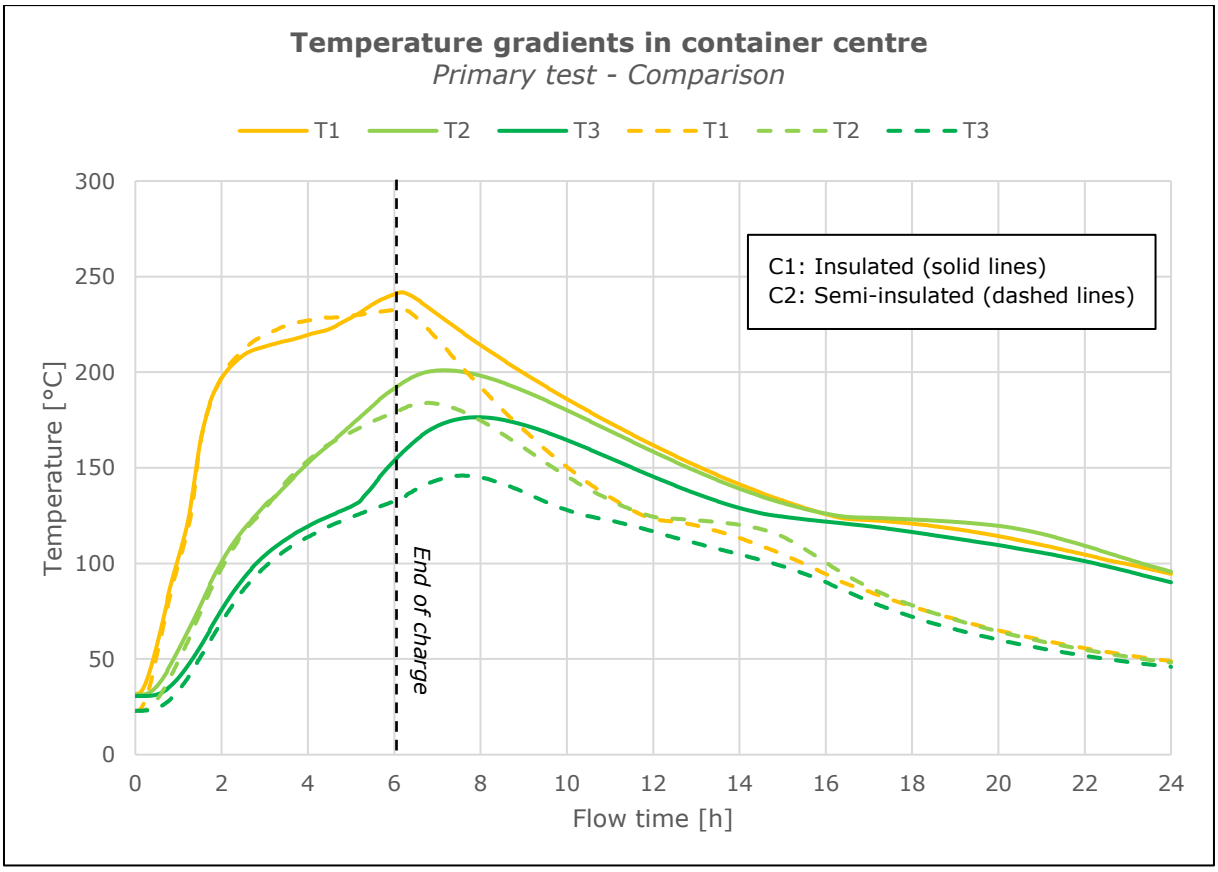


**Figure 4-11:** Primary test; comparison of temperature gradients in container centre

During charge in C1, the typical phase change curve is most visible for T3 with a markedly change in temp gradient at about 130 °C (at 5 hours flow time) which fits well within the melting temperature range. The reason for a more gliding transition for T1 and T2 might be due to the low thermal conductivity (heat accumulates, fast melting), consequently with large temperature difference between the layers. Then, when dT is larger, there is more heat loss to the above layers and T1 stabilizes. For C1, when T3-layer has melted, its temperature gradient gets steeper, dT to T1 decreases and then T1 increases faster. Note that the thermal oil can affect the heat transfer in the pcm.

For C2, a similar pattern is seen, only delayed due to more heat loss from side wall and possibly the slightly lower initial temperature. Also, T3 continues to increase for almost 2 hours after charge end, due to higher temperatures in lower layers and the stored heat in heating plate. The T3 gradient also becomes steeper before it flattens out just below 150°C, indicating that the upper layer also has melted, utilizing more of the latent heat. However, a visual check after 8 hours flow time was done, where the pcm on top (which was in air contact) had not melted completely, as it was still white and opaque, opposed to the clear and transparent form molten HDPE has.

Note that a slight increase in the slope for T1 is seen at about 1-hour flow time (also visible in fig. 4-7 at 2 hours flow time), which is likely due to the lower thermal conductivity in the melted pcm. Hence, the heat transfer through layer is slowed down, resulting in larger heating of the layer.

It also seems strange that T1 for C2 surpasses T1 for C1 just after 2 hours flow time, when C1 is better insulated. However, T1 is placed just above container bottom and C2 has larger heat load due to larger heat loss. Further, there is slow heat flow through the pcm (due to low k), so it's reasonable that T1-layer gets hotter during C2.

During discharge, the temp gradient, notably for T1, is steeper for C2 due to larger heat loss, consequently solidification occurs earlier in the process. This is also affected by the lower temperature at charge end, with less sensible cooling before solidification temperature is reached.

During solidification, the temperatures (notably T2, which is at the pcm core) stabilizes at lower temperature (122 °C) than the melting temperature (134 °C), which clearly displays the supercooling effect as discussed in Chapter 2.1. It is also seen from fig. 4-11 that the temperature difference between the TC (for each cycle) is much smaller during discharge compared to charge. This is probably due to smaller driving forces and more time for heat to dissipate in the pcm. Also note that T2 (pcm core) is the highest temperature at end of solidification.

Regarding the typical phase change curve for solidification, T3 now has a more gliding curve, as it loses heat faster to air inside the container. Temperature differences within the pcm is now smaller, while T2 loses heat more slowly (due to low k in surrounding pcm) and the phase change curve is more visible.

Further, a similar pattern as seen during the filling stage, with large temperature differences within the pcm at charge end, appeared in the primary test. Temp difference between T1 and T3 is approx. 90°C for C1 and 100°C for C2, which indicates that there is only conduction heat transfer in the pcm, whereas this difference should be smaller if free convection occurred (mixing of layers). This is probably due to the rubbery state of the pcm (not completely liquid), where the viscous forces are too high for free convection to

set, which consequently limits the heat transfer in the pcm. On the other hand, the pcm is melted and the latent heat is stored.

### 4.3.2 Phase change front

In an experimental test, especially in this case with few measuring points in the PCM, it's difficult to estimate the liquid fraction. A numerical simulation showing similar temperature development could be used for validation of the liquid fraction. Unfortunately, as mentioned, this was done with wrong boundary condition at container bottom and was not applicable for comparison.

Further, because of the large temperature differences throughout the PCM (low thermal conductivity and no convective effect), there will be significant difference in density as well, which is a function of temperature. Another factor, when the pcm is solid (with higher density), it contracts away from container walls, leaving air gaps as shown in fig. 4-8. Hence, even though knowing the filling level, this contraction makes it hard to estimate the PCM volume.

However, the height of the PCM volume seemed constant, while the contraction accounted for changes in density. This way, the phase change front can be traced based on the TC position. The height (filling level) was estimated to 0.065 m as the top layer of PCM covered the T3 cannula pipe. Note that the estimated filling level is the same value as for the height of T3 in fig. 3-8 and might be confusing, but the thickness of container bottom plate is not included in the calculation of volume fraction, just to clarify.

To track the phase change front, the parameter *VF*, which is the height-based volume fraction of melted pcm, is shown in equation *(4.1)* below:

$$VF = \frac{H_i}{H_T} \qquad (4.1)$$

Where $H_i$ is the height of the respective TC above the container bottom inside surface and $H_T$ is the total height of the PCM volume (filling level).

During charge, when T1=134°C, all the PCM up to this level is melted, which then gives *VF*=0.15 and so on, as shown in Table 4.1. Further, no pcm has melted before T0 reaches 134°C, hence *VF*=0 during the first half hour.

During solidification, the phase change process is somewhat different compared to melting (heated from bottom and up), where the pcm solidifies from the container walls and inwards. This is seen in fig. 4-11 where both T1 and T3 is lower than T2, hence both the top and bottom layer becomes solid before the core. So, when T3=122°C, the top layer has solidified, giving a *VF*=0.92 and so on. The calculated values for *VF* are plotted in fig. 4-12, which includes intermediate points between the TC as there was only conduction within the pcm, assuming a linear temperature gradient.

**Table 4.1** – Volume fraction of melted PCM during charge

| TC position in PCM | Charge |
|---|---|
| $H_1$=0.010 m | 0.15 |
| $H_2$=0.035 m | 0.54 |
| $H_3$=0.060 m | 0.92 |
| Filling level: $H_T$=0.065 m | |

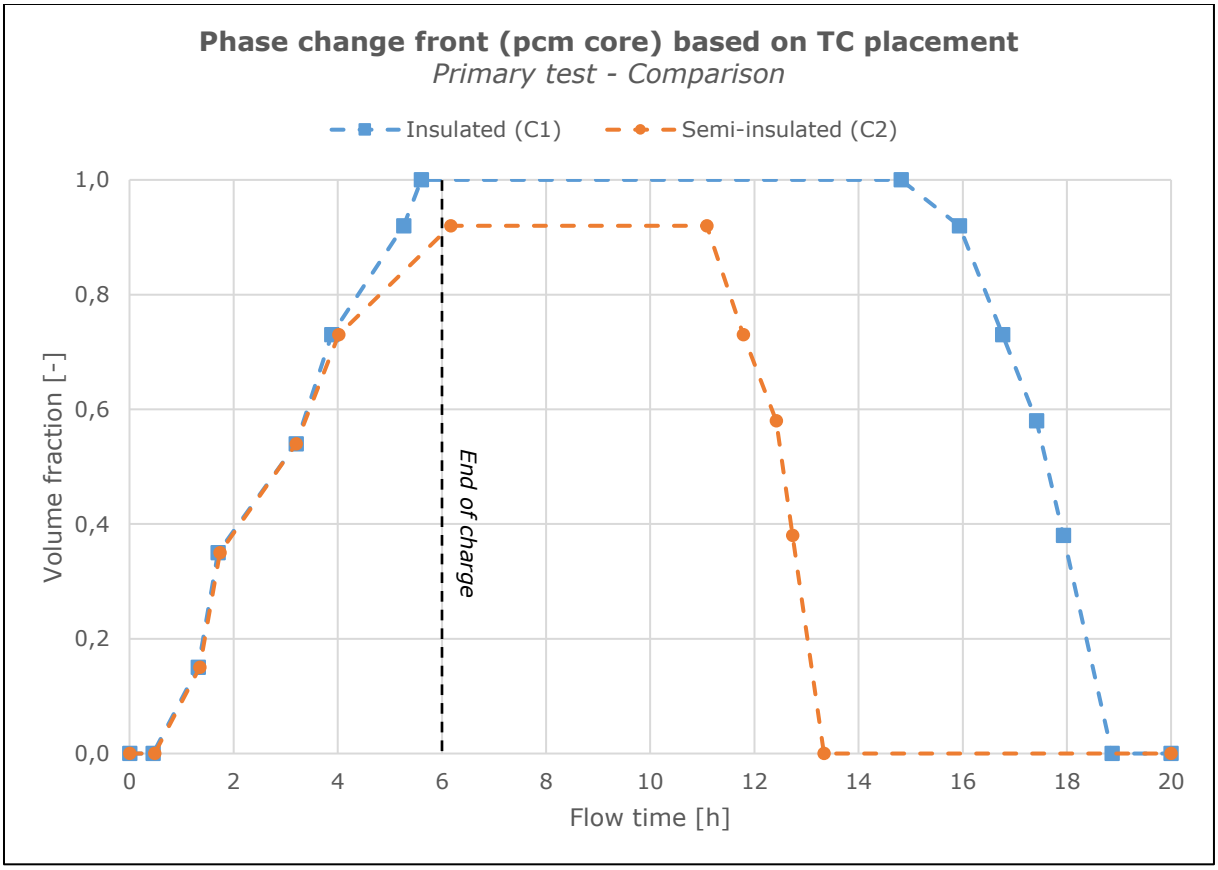


**Figure 4-12:** Phase change front at core of PCM, based on TC placement

This method for tracing the phase change front is limited due to few measuring points and the uncertain calculation of *VF*, as it is based on an estimated filling level. See Appendix C for the uncertainty analysis. However, it provides a comparison between the two cycles.

During charge, the *VF* gradient would likely be somewhat steeper due to heat transfer from container walls (this pcm melts sooner than the core), before becoming gentler as it approaches 1. During discharge, *VF* would start to decrease sooner in process due to heat loss from all sides, while the core is the last part to solidify (solidification front moves inwards). Hence, the slope of *VF* would be gentler and the real solidification time is much longer.

Apart from this, at least the calculated *VF* gives an indication on the phase change process at the container centre, most notably the melting time and the difference between the cycles. As seen from fig. 4-12, almost the same development in melt front until 4 hours flow time, then C2 slows down. This is when the heat loss is the largest, especially for C2 where the side wall insulation was removed.

A visual check during C1 proved that all pcm had melted, hence *VF*=1, whilst for C2 some pcm in the top layer did not melt. So, based on the available data it could only be assumed that pcm up to T3 had melted, with a *VF*=0.92. This is further used in calculation of stored heat in pcm, where only 92 % of the latent heat were utilized during C2.

During solidification, the most notable differences in fig. 4-12 is the slightly steeper curve during C2 and that it occurs earlier in the process, which makes sense due to larger heat loss. This also corresponds with the temperature gradients in fig. 4-11, where the core (T2) solidifies at approx. 11-13 hours for C2 and 16-19 hours for C1. Table 4.2 shows the phase change time for the pcm core and as mentioned, the solidification time for entire pcm is significantly longer. The core melting time is based on the time from T1=134°C until T3=134°C, and T3=122°C to T2=122°C for the solidification time.

Although Table 4.2 gives a distorted impression between melting and solidification time, it displays the difference between the cycles, where C1 melts faster and solidifies slower due to less heat loss.

**Table 4.2** – Melting and solidification time for PCM core

| | **C1** | **C2** |
|---|---|---|
| Melting time [min] | 237 | 289 |
| Solidification time [min] | 176 | 135 |

Note: Since the PCM was wetted with thermal oil (to avoid oxidation), this can affect all parameters including phase change temperatures and time, heat transfer in pcm, energy stored and ultimately the composition (if any chemical reactions). However, the thermal oil has similar properties (also being a hydrocarbon-based fluid) as HDPE and proved stable except some evaporation during C1 charge end.

### 4.3.3 Heat balance

Since the container was half-full during the primary test, the upper TC were rather used for additional temperature measurements on the test rig surfaces to get a better estimate of the heat loss. TC was placed at intermediate points on the surface to get an average temperature, as there likely were temperature gradients along the surface as well.

The heat loss was calculated for each surface with its respective TC, based on equation *(3.5),* and then summed together to get the total heat loss, as shown in fig. 4-13. The most notable difference between the cycles was the radiation heat loss for C2 (eq. *(3.6)* included for the side wall), whereas radiation during C1 was assumed negligible due to the insulation was covered with Aluminium-foil which has very low emissivity (ε=0.04). At charge end, the side wall surface temp (container) was 122°C for C2, whilst the side wall surface temp (insulation) was only 48°C during C1. Hence, the convective heat loss during C2 was larger as well.

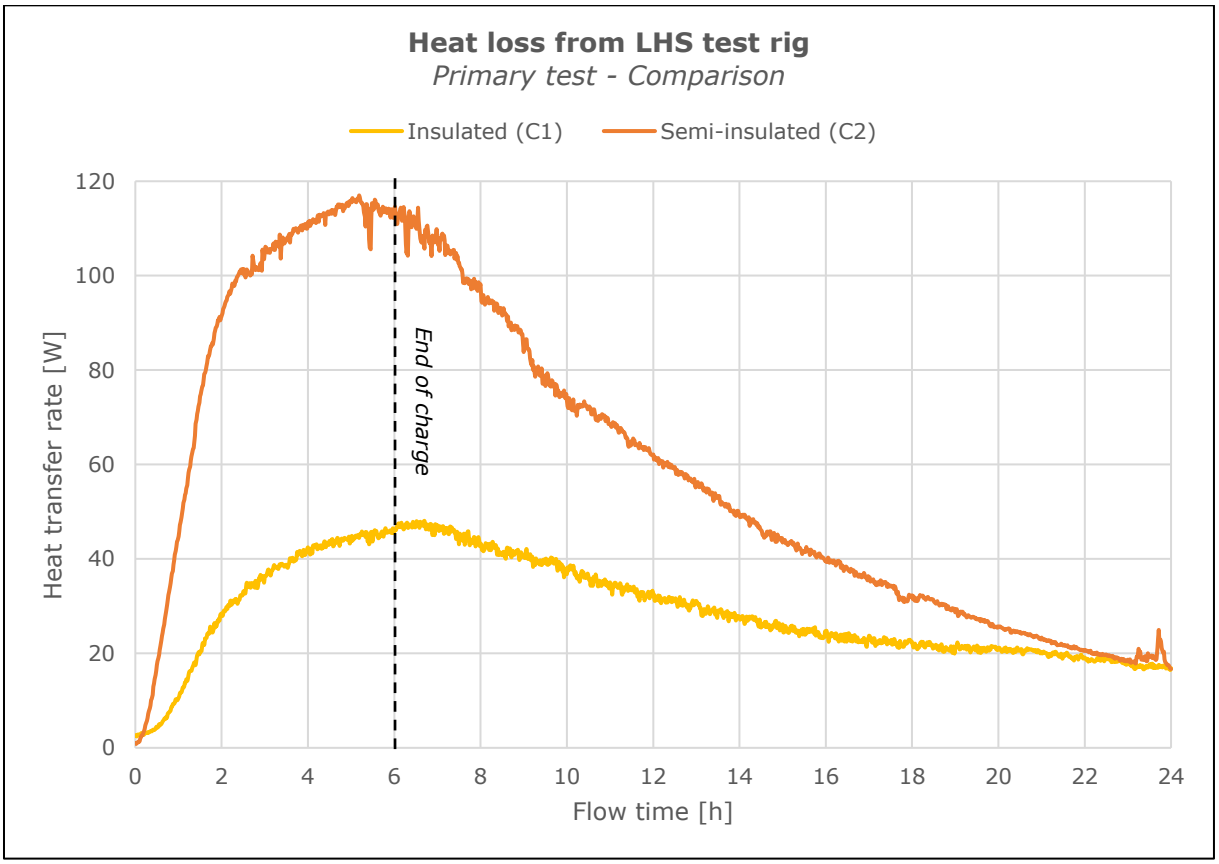


**Figure 4-13:** Heat loss from test rig; comparison between primary test cycles

As seen in fig. 4-13, there were some disturbances during C2. Most notably at charge end, the tape that was holding T12 in place, loosened due to the hot container wall. At end of discharge (24 hours), T13 at the insulation tray was hit by sunlight, increasing its temperature. Another disturbance might have been opening of the lab door, supplying fresh and cooler air.

At charge end, note that the heat loss for C2 is almost 120 W and the heat load is 150 W (fig. 4-10), thus net heat flow of 30 W to the pcm. This seems reasonable as the pcm was heating slowly (gentle gradients in fig. 4-11). Compared to C1, the heat loss at charge end is about 50 W while the heat load is 100 W, with net heat flow of 50 W to the pcm. Hence, slightly more than during C2, which concurs with the steeper gradients (faster heating) in fig. 4-11.

Further, the heat released is calculated by multiplying the heat transfer rate by each minute flow time, and then summed together for the first 6 hours during charge and then for the next 18 hours during discharge. This is equivalent to the area under the graph in fig. 4-13 and has the unit Wh. The same was done to find the total heat input, which corresponds with the area under the heat load in fig. 4-10.

Charge end is a reasonable time for comparison between the two cycles, as it shows the potential of LHS system when combustion is finished. Then the heat load is turned off and the PCM has its max temp. The method used to estimate the heat stored in the pcm is based on the total heat balance of the test rig, where the heat load must equalize the heat stored and heat released. Then, a control calculation of the stored heat in the pcm was done for validation, using eq. *(4.2)* with average values for specific heat, with the unit for stored heat changed to kWh.

$$Q, pcm(control) = m_{pcm}\left[\left(c_{p,solid}(T_m - T_\infty)\right) + L + \left(c_{p,liq}(T_{av} - T_m)\right)\right] \qquad (4.2)$$

The temperature data are listed in Table 4.3, while the different material properties are found in Chapter 3. The results with respective uncertainties are listed in Table. 4.4.

**Table 4.3** – Temperature data at charge end

| $T_\infty$=22°C | **C1** [°C] | **C2** [°C] |
|---|---|---|
| Heating plate (T0) | 275.5 | 274.8 |
| Container bottom plate | 270 | 270 |
| Fyrewrap average | 120 | 100 |
| Skamolex plate | 270 | 270 |
| Foam plates | 40 | 40 |
| PCM average, $T_{av}$ | 205 | 177 |

Several assumptions were made regarding the stored heat in the system, as both the container and the insulation stores heat. The container bottom plate is assumed to have somewhat lower temperature than the heating plate, while the Fyrewrap average temperature is the mean value between the pcm and the insulation surface temperature, as there is a steep gradient through the insulation. Similar for the foam plates, only between the heating plate and the table, based on the U-value calculated by hand. Further, the heating plate posed a significant part of the total heat stored in the system, due to its large thermal mass. Although not a part of the LHS concept (pcm and container), it must be included with respect to the heat balance.

Regarding the heat released, the loss to air was assumed to be somewhat larger due to powerful ventilation above the rig, whereas a small decrease in the air pressure pulls in air from the sides, resulting in some forced convection. Hence, the heat transfer coefficients listed in Table 3.6 should be larger. To simplify, the total heat loss during C1 was increased by a factor of 1.2 to compensate this effect. For C2, the factor was reduced since most of the increased heat loss is due to radiation, which is not affected by the ventilation. Based on hand calculations on the ratio between convective and radiative heat loss, the factor was set to 1.1.

The heat loss to table is excluded from fig. 4-13 due to unknown properties of the material used inside the tray and furthermore the small values, but an estimate is included in the heat balance.

**Table 4.4** – Heat balance at charge end

| **Component** | **C1** [kWh] | **C2** [kWh] |
|---|---|---|
| Q,input | 1.4 ± 2% | 1.62 ± 2% |
| Q,heating plate | 0.357 ± 0.005 | 0.356 ± 0.005 |
| Q,container | 0.072 ± 0.004 | 0.072 ± 0.004 |
| Q,insulation | 0.207 ± 0.013 | 0.182 ± 0.010 |
| Q,loss air | 0.223 ± 0.003 | 0.579 ± 0.006 |
| Q,loss table | 0.027 ± 0.001 | 0.027 ± 0.001 |
| Q,pcm (heat balance) | 0.514 ± 0.032 | 0.404 ± 0.035 |
| Q,pcm (control) | 0.441 ± 0.021 | 0.383 ± 0.022 |
| *Nominal value ratio* | *86 %* | *95 %* |

The control value for Q,pcm in Table 4.4 is lower than the heat balance estimate of Q,pcm for both cycles. This is also expressed by the ratio, which is the nominal control value relative to the heat balance value. The difference can be due to the simple control calculation based on average values for temperature and specific heat, as these factors vary significantly throughout the pcm. The average temp for pcm can also be affected by conduction in the cannula pipes. Further, the stored heat in the test rig can be affected by uncertain material properties, nor is there control on all heat losses which is also based on average values.

In other words, the calculations are uncertain. Table 4.5 shows that the difference in Q,pcm for C2 can be justified by the uncertainties, with good overlap in the values. For C1, there's still a small gap between the values, most likely due to simplifications in the method or mistakes made in the calculations. The uncertainty analysis can be found in Appendix C.

**Table 4.5** – Uncertainty of heat stored in PCM

| | **C1** [kWh] | **C2** [kWh] |
|---|---|---|
| **Heat balance** | | |
| Q,pcm ± ΔQ,pcm | 0.514±0.032 | 0.404±0.035 |
| Q,pcm (min) | 0.482 | 0.369 |
| **Control calc** | | |
| Q,pcm ± ΔQ,pcm | 0.441±0.021 | 0.383±0.022 |
| Q,pcm (max) | 0.462 | 0.405 |
| *Percentage ratio* | *96 %* | *110 %* |

Further, the effect of the LHS system is displayed in fig. 4-14, where a substantial part of the heat load is stored during charge, for later release. As seen in Table 4.4, the heating plate stored almost as much heat as the pcm, hence the portion of latent heat storage is smaller for this experiment compared to the concept integrated on a wood stove. However, fig. 4-14 is meant to show the concept's purpose, with a more stable heat release from the wood stove.

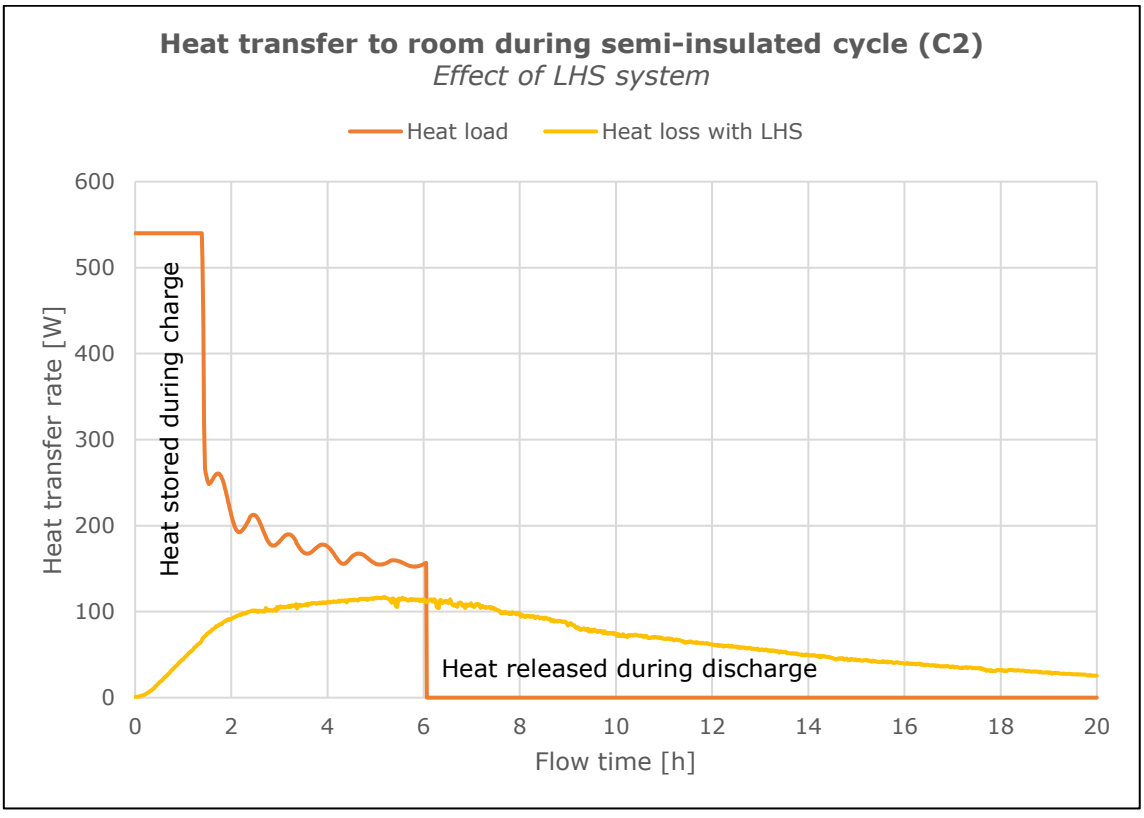


**Figure 4-14:** Effect of LHS system on heat transfer to room

Further, a graphical overview of the heat balance is presented in fig. 4-15 and can be interpreted as the LHS thermal performance. The heat released is the combined heat loss to air and table during charge, while the heat stored (in all system components) represents the heat to be released during discharge.

Note that for each cycle, the heat released and the heat stored equals the heat input. When comparing the heat balance between the cycles, the difference in heat stored and heat input also match the difference in heat released. For C2, the heat input is larger and the heat stored is less, so this extra heat must have been lost.

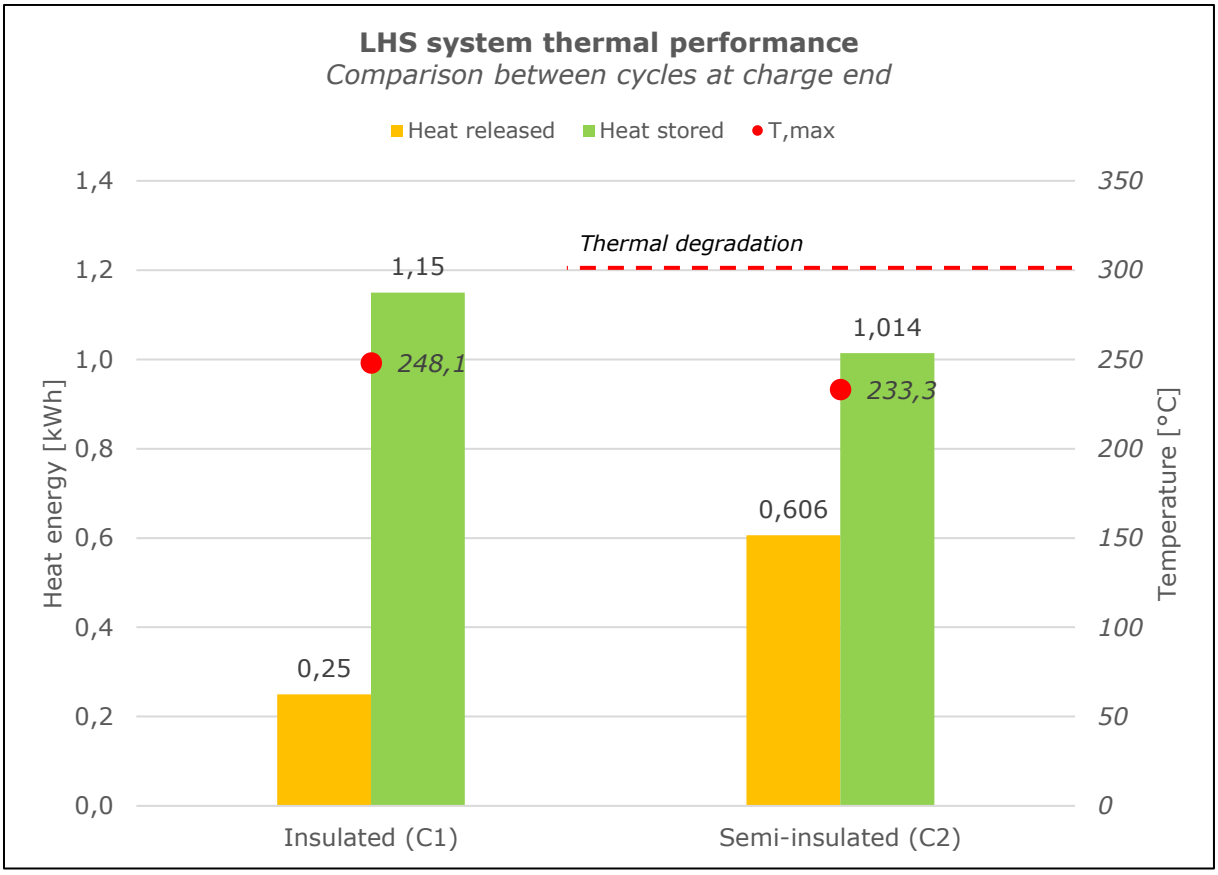


**Figure 4-15:** LHS system thermal performance during realistic combustion duration

In order to dampen the peak effects from the wood stove, it's desirable to have most of the heat release during discharge. As C1 was completely insulated, C2 gives the best impression of the current design's performance. To approach the pcm storage capacity in the complete concept, with a coaxial system (x4), full container (x2) and assuming similar temperature development, the magnitude of stored heat in the pcm would be 3.232 kWh. This is about half of the 6 kWh which is desired to store, as mentioned in Chapter 3.1.

The danger for thermal degradation was avoided during the experiment, due to the temperature control in the heating plate. However, for the final concept integrated on a wood stove, where there is no such control, this could pose a risk for destroying the pcm and severely affect the performance and durability of the LHS system.

### 4.3.4 Effective thermal conductivity

Even though the heat balance seems reasonable, an estimate of the thermal conductivity in the pcm was done to validate the results. Due to the large temperature differences within the pcm and the assumption of no convection, the effective conductivity should be close to literature values, as listed in Table 3.1.

The estimation was based on Fourier's law of conduction (eq. 4.3), assuming one-dimensional conduction in the pcm due to uniform heating from the bottom plate:

$$q_{pcm} = kA\frac{\Delta T}{\Delta x} = \left(\frac{k}{\Delta x}\right) A\Delta T = U_{eff} A\Delta T \tag{4.3}$$

$$\frac{1}{U_{eff}} = R_{eff} = \sum_{i=1}^{n} R_i = \frac{\Delta x_{cu}}{k_{cu}} + \frac{\Delta x_{steel}}{k_{steel}} + \frac{\Delta x_{pcm}}{k_{pcm}} \tag{4.4}$$

$$k_{pcm} = \frac{\Delta x_{pcm}}{\left(\frac{A\Delta T}{q_{pcm}}\right) - \left(\frac{\Delta x_{cu}}{k_{cu}} + \frac{\Delta x_{steel}}{k_{steel}}\right)} \tag{4.5}$$

Where the efficient heat transfer value, $U_{eff}$, from the heating plate to pcm can be expressed as the sum of all the individual thermal resistances, $R_i$, as given in eq. *(4.4)*. The estimate of the effective thermal conductivity in the pcm, $k_{pcm}$, is then calculated using eq. *(4.5)*.

Further, $q_{pcm}$ is the net heat flow in pcm, $k$ is the thermal conductivity, $A$ is the heat transfer area (container bottom area), $\Delta T$ is the temperature difference between the heating plate and the respective TC in the pcm, and $\Delta x$ is the distance between heating plate and the thermocouple. Note that $\Delta x_{cu}$ was set to half the thickness of the heating plate, as the heat load is applied internally. However, the combined thermal resistance from the heating plate and container bottom, $R_{cu,steel}$, is very small compared to the pcm resistance, assuming complete contact between the surfaces. The container bottom was not perfectly plane due to buckling caused by heat when being welded, so a small thermal resistance between the plates is likely. To simplify, this was neglected.

The thermal conductivity changes throughout the process, as it is a function of temperature. It was evaluated at charge end, both for conformity with the other analysis and due to this is when the system is closest to steady state. Table 4.6 lists the process data used for the calculation, whilst the results are shown in Table 4.7.

**Table 4.6** – Process data at charge end, for calculation of PCM effective thermal conductivity

| *T0=275°C, $A_{bot}$=0.045 $m^2$, $R_{cu,steel}$=0.000455 $m^2K/W$* | | | |
|---|---|---|---|
| | | **C1** | **C2** |
| | *Position ($\Delta x_{pcm}$)* | | |
| T1 | 0.010 m | 240.8 °C | 232.7 °C |
| T2 | 0.035 m | 191.5 °C | 179 °C |
| T3 | 0.060 m | 153.7 °C | 132.6 °C |
| q,in (heat load) | | 106.4 W | 155.3 W |
| q,loss | | 55.3 W | 114.1 W |
| q,pcm | | 51.1 W | 41.2 W |

Note that kelvin (K) is used in the unit for conduction, whilst centigrade (°C) is the unit for the temperature measurements. This is due to the temperature data were logged in centigrade, while the unit for thermal conductivity is preferred in absolute temperature (kelvin). However, when calculating temperature differences, it makes no difference regarding the result, as the magnitude is the same.

Further, the relative uncertainties of the thermal conductivity are listed in Table 4.7 to better point out the differences, as the absolute uncertainties are similar in value. The uncertainty analysis is discussed in Appendix C.

**Table 4.7** – PCM effective thermal conductivity at charge end

| *k,pcm ± Δk,pcm*<br>**TC position** | **C1**<br>[W/m·K] | **C2**<br>[W/m·K] |
|---|---|---|
| T1 | 0.33 ± 12.1 % | 0.22 ± 13.6 % |
| T2 | 0.48 ± 4.2 % | 0.34 ± 5.9 % |
| T3 | 0.56 ± 3.8 % | 0.39 ± 2.6 % |

The values for C1 are somewhat large since all temperatures indicate that the pcm is melted, compared to the literature value of 0.21 W/(m·K) for liquid state. The uncertainty for the calculated values does not cover the entire gap to this value, except for T1 during C2. This deviation can be due to that the pcm is still heating, as seen in fig. 4-16, with slowly increasing temperatures at charge end. Hence, some of the heat flow in the pcm goes to heating, thus the heat transfer rate through the pcm is somewhat lower. For the calculation, the U-value should then be lower, the thermal resistance higher and the thermal conductivity would be lower.

When comparing the two cycles, the values for C2 in Table 4.7 are closer to the literature value. Based on the difference in temperature gradients at charge end, shown in fig 4-16, the pcm in C1 (better insulated) has steeper gradients and is heating more than during

C2, which has more heat loss and is closer to steady state. The gentler gradients for C2 is better for estimating the thermal conductivity, where larger part of the heat flow is transferred through the pcm (opposed to heating the pcm), which is what the conductivity is a measure of. Note that the temperature gradient for T1 during C2 is the gentlest, which corresponds with the most accurate value in Table 4.7. Also, the T3 temperature for C2 is at the melting point, so an intermediate value between the theoretical values (0.55>0.39>0.21) seems like a good estimation.

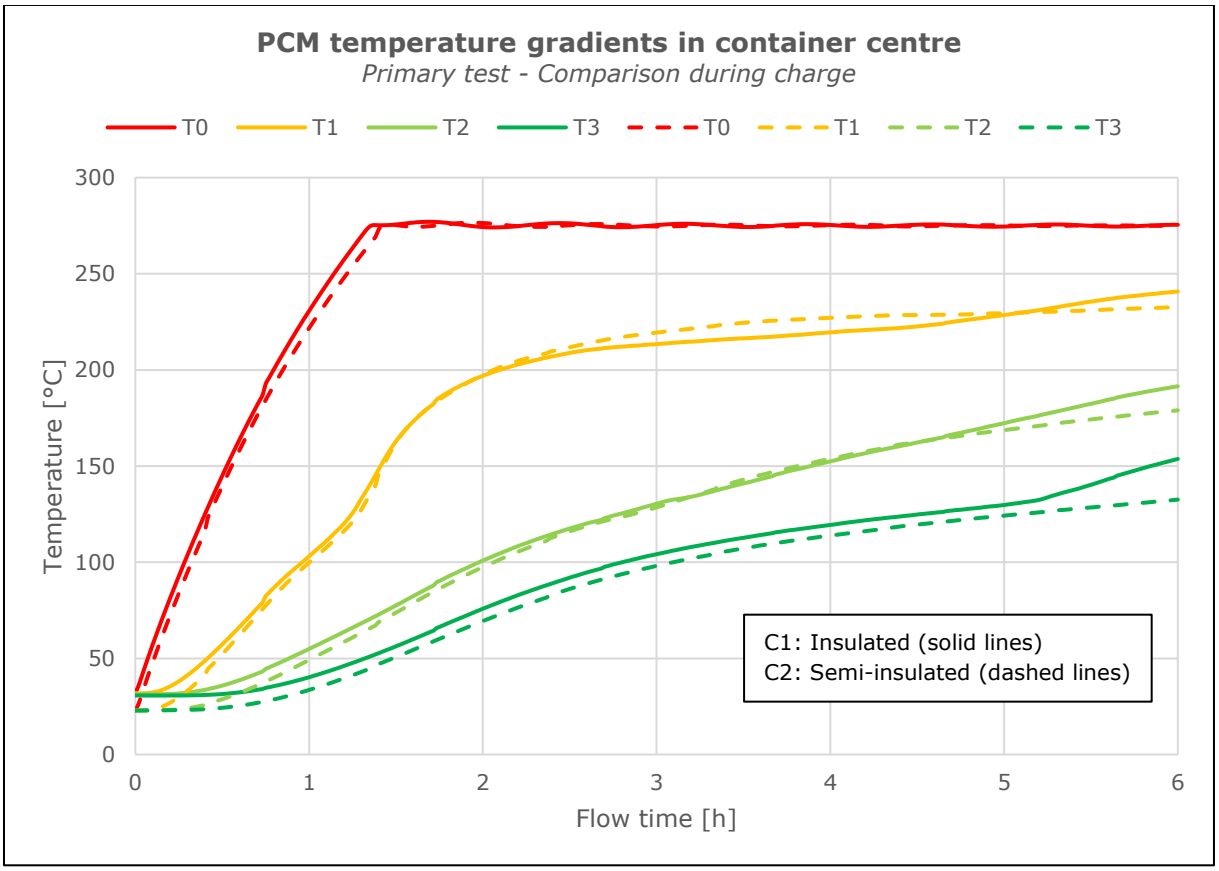


**Figure 4-16:** Primary test; temperature gradients at container centre during charge

Based on the values for the effective conductivity, which all are close to the theoretical values, and the large difference between the temperature gradients, this indicates that there is no free convection in the pcm. If it was, far larger values for $k_{pcm}$ would be expected as the thermal resistance would be much lower and the U-value higher, due to the convective effect. Also, the temperatures at charge end should be more consistent (closer in value), as convection would mix the pcm layers. Further was there no flow visible from the top opening, nor was it possible to stir the pcm. Hence, it was in a rubbery and viscous state at charge end. Since there is only conduction heat transfer in the pcm, the large temperature differences are reasonable due to the low conductivity of the material.

In other words, heat transfer enhancement is needed to ensure melting of all pcm, especially in the upper layer for C2, which is the cycle that gives the best impression of the concept.

### 4.3.5 Summary of discussion

The primary test consisted of two different cycles, the first (C1) where the test rig was completely insulated whilst the side wall insulation was removed during the second (C2). Several parameters were analyzed to compare the two cycles; temperature development, phase change front, heat balance and estimation of thermal conductivity.

The temperature development during C2 showed that the pcm reached lower average temperature at charge end, with larger heat load, compared to C1. This seemed reasonable as the heat loss during C2 was more than doubled due to less insulation. The temperature difference within the pcm proved to be large, which indicated absence of free convection. A visual check proved that some pcm in the top layer did not melt for C2, thus slightly less latent heat was stored. Further, the melting was slower and the solidification was faster for C2, due to the increased heat loss. The heat balance for the test rig was used to estimate the stored heat in the pcm, which then was compared to a control value based on the heat increase in the pcm. Though somewhat different values, likely due to simplifications in the method, it could be explained by the uncertainties in the calculations for C2. Lastly, to validate the results, an estimate of the pcm effective thermal conductivity was carried out, which proved reasonable values for the material and further supported the assumption of only conduction heat transfer within the pcm.

Regarding other properties of the pcm, the latent heat is suspected to be somewhat lower than the theoretical value used in the calculations, consequently resulting in less heat stored in the pcm. Further, the dynamic viscosity is likely much higher as the melted pcm had a rubbery consistency. The value used was similar to water, where it should rather be closer to that of syrup.

As the final concept has no insulation, C2 can be viewed as the best prediction for the LHS concept thermal performance. Due to the design of the experiment, the heating plate posed a large thermal mass with sensible heating, storing significant portions of the heat load. However, when evaluating the heat stored in the pcm, it was assumed to store about half of the desired amount, when scaled up to the final concept. Further, heat transfer enhancement (HTE) in the pcm can help increase the heat stored, especially when the convective effect is absent. This would also result in faster melting by better distribution of the heat flow to the pcm, and possibly reduce the risk of overheating the pcm bottom layer in the container, avoiding degradation.

HTE would also help to release the heat during discharge, as the pcm temperature at discharge end was still larger than the ambient. Hence, when the next combustion cycle is initiated the following day, the risk of overheating the pcm is higher. However, the final concept does not have the large thermal mass of the heating plate, which is well insulated. Though the wood stove itself poses such a thermal mass, it is not insulated. Thus, the LHS unit is assumed to reach ambient temperature.

For this experiment, the temperature control in the heating plate assured that degradation temperature was not reached. However, for the final concept integrated on a wood stove, degradation might affect the performance and durability of the LHS unit. This proved to be a weakness in the experimental design, as part of the goal was to test the concept for max heat flux to the container bottom, opposed to a constant temperature which was the case for the test.

# 5 HEAT TRANSFER ENHANCEMENT

## 5.1 Fin analysis

This chapter presents a brief analysis of heat transfer enhancement (HTE) in the pcm, using stainless steel fins inside the container. The initial analysis was based on the results from the project work [7], with free convection in the melted pcm. Due to the results from the experimental test, with only conduction present, the analysis had to be changed, as this would affect the fin design.

Though free convection is absent, the results from the project work indicated that applying fins to the container bottom and top improved the thermal performance of the concept, both with respect to faster melting, more heat stored in the pcm and more efficient heat release during discharge. However, this was based on a simplified numerical simulation, so the fin geometry should be investigated in more detail. To find the fin arrangement best suited for the concept, the following calculations are based on equations for heat transfer from extended surfaces, as described by Incropera et.al. [25].

To determine the fin length, $L_f$, the temperature gradient throughout a rod fin is investigated, as given in eq. (5.1). This equation is also valid for fins with a uniform cross-section, as imagined for the container.

$$T_f = T_\infty + (T_b - T_\infty)e^{-m_f L_f} \tag{5.1}$$

$$m_f = \left[\frac{hP}{kA_c}\right]^{\frac{1}{2}} \tag{5.2}$$

Where $T_f$ is the temperature at fin tip, $T_\infty$ is the temperature of the surrounding fluid, $T_b$ is the base temperature of the fin, $m_f$ is the corrected convective fin tip and $L_f$ is the fin length. Equation *(5.2)* is the expression for $m_f$, where $h$ is the convective heat transfer coefficient in the fluid (pcm), $P$ is the perimeter of the fin's cross-sectional area, $k$ is the thermal conductivity of the fin material and $A_c$ is the cross-sectional area of the fin.

Further, these equations are valid when assuming steady state condition, uniform temperature profile across the fin, constant material properties, that radiation is negligible and infinite fin length such that $T_f(L_f \rightarrow \infty) = T_\infty$ (fin tip temperature equals the surrounding temp). Although this is not the real case, these simplifications can be used to get an impression of the fin performance.

Further, it is assumed favourable that the bottom fins are also connected to the pipe wall, as some heat transfer from the exhaust gas is expected in the final concept (charge, heat in). The top fins should also be in contact with the outer side wall of the container, which will enhance the heat transfer during discharge (heat out). However, the side wall contact is disregarded for this analysis, as there would be some conduction through the walls affecting the fin temperature profile.

The fin width is set to $w$=0.1m such that the fins extend approx. 60 % into the pcm volume (distance between pipe and outer side wall). Changes for this parameter could also be analysed, but it was selected as a starting point.

In the project work [7], it was suggested that the bottom and top fins should be alternating, with 14 fins each for the coaxial concept. For the test container, which is a 90-degree slice, this suggestion was adjusted to include 4 fins each. This number seemed reasonable as too many fins will increase the system weight and further displace the pcm.

The following analysis is based on the change in fin length and thickness, and how it will affect the heat transfer. Due to the container was only half-full of pcm and insulated on the top surface, the emphasis is on the bottom fins. Further, since there is only conduction heat transfer in the pcm, $h$ in eq. *(5.2)* is substituted with the U-value $U_f$ which is based on the thermal resistance in the pcm. Note that this value will change throughout the process, as it is a function of temperature ($k$ changes). For this selected number of fins, the distance between the fins is approx. 50 mm, such that the heat transfer from the fins dissipates through a layer of pcm with thickness set to half this distance (intermediate point between the fins). The calculation is listed in Table 5.1.

**Table 5.1** – Calculation of U-value between fins and PCM

| | **Value** | **Unit** |
|---|---|---|
| Layer thickness | 0.025 | m |
| $k_{pcm}$ (solid) | 0.55 | W/(m·K) |
| $R_f$ (resistance) | 0.045 | (m$^2$·K)/W |
| $U_f$ | 22 | W/(m$^2$·K) |

During charge, $T_b > T_\infty$ as heat is flowing from the bottom surface and into the pcm. $T_b$ is assumed somewhat lower than T0 (heating plate) due to the gradient through the container bottom and $T_\infty$ is the average value in the pcm, as there was large temperature difference within the pcm. The corrected convective fin tip, $m_f$, expresses how rapid the temperature decreases along the fin length and is calculated from eq. *(5.2)* and shown in Table 5.2 for different fin thickness:

**Table 5.2** – Fin parameters during charge

| *$h=U_f$=22 W/m$^2$K ; k=15 W/m·K ; $T_b$=250°C ; $T_\infty$=200°C* | | | | |
|---|---|---|---|---|
| **Fin thickness** | **1.5 mm** | **3 mm** | **5 mm** | **Unit** |
| $P$ | 0.203 | 0.206 | 0.21 | m |
| $A_c$ | $1.5\cdot10^{-4}$ | $3\cdot10^{-4}$ | $5\cdot10^{-4}$ | m$^2$ |
| $m_f$ | 44.6 | 31.7 | 24.8 | m$^{-1}$ |

Then, the fin tip temperature $T_f$ is calculated as a function of the fin length, using eq. *(5.1)* and the data in Table 5.2. The results are displayed in fig. 5-1. The dashed line shows the effect of changing the fin material to aluminium, which has much higher thermal conductivity (also lower density), consequently resulting in more efficient fins.

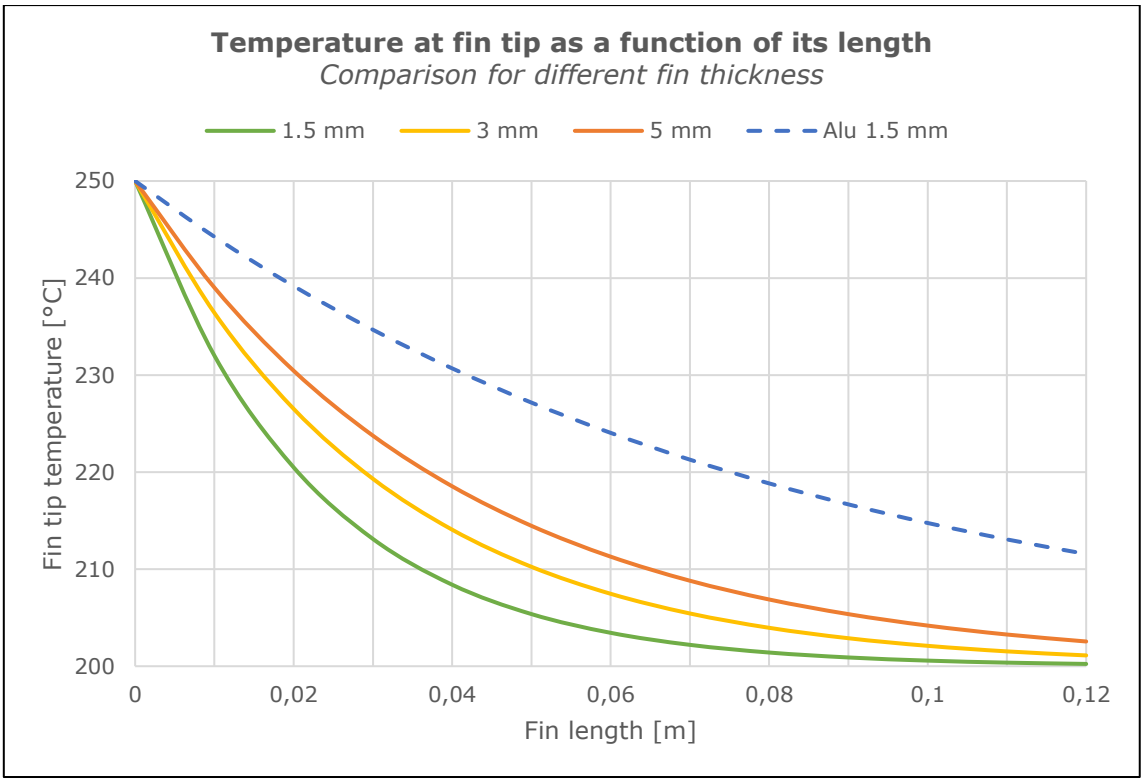


**Figure 5-1:** Fin tip temperature for container bottom fins

As seen in fig. 5-1, the fin tip temperature decreases as the length is increased, implying that the fin gets less efficient the longer it is. Thus, there should be at least 10°C difference between the fin tip and the pcm for any significant heat transfer to occur at the fin tip. When increasing the fin thickness, the length can also be increased, e.g. for thickness of 1.5 mm, the length should only be 30 mm, whilst for 5 mm thickness it can be 60 mm. Additional length would be excessive, as it would not contribute to more heat transfer, rather only increasing the weight.

Although it should be mentioned that fins are most efficient when $h$ is small, as they increase the heat transfer area. Further, to compare the heat transfer from the fin and its coherent efficiency, the following equations [25] were used.

$$\eta_f = \frac{\tanh\left(m_f L_{cf}\right)}{m_f L_{cf}} \tag{5.3}$$

$$L_{cf} = L_f + \frac{t}{2} \tag{5.4}$$

The fin efficiency $\eta_f$ is expressed in eq. *(5.3)* and *(5.5)*, where $L_{cf}$ is the characteristic fin length given by eq. *(5.4)* with $t$ being the fin thickness. $A_f$ is the surface area of the fin, which can be calculated using eq. *(5.6)*. Note that $q_{f,max}$ represents the theoretical max heat transfer, if the entire fin is at the base temperature $T_b$.

$$\eta_f = \frac{q_f}{q_{f,max}} = \frac{q_f}{hA_f(T_b - T_\infty)} \tag{5.5}$$

$$A_f = PL_{cf} \tag{5.6}$$

Then, when using these equations and data from Table 5.2, both the fin efficiency and the heat transfer from the fin are calculated as function of the fin length. The results are shown in fig. 5-2.

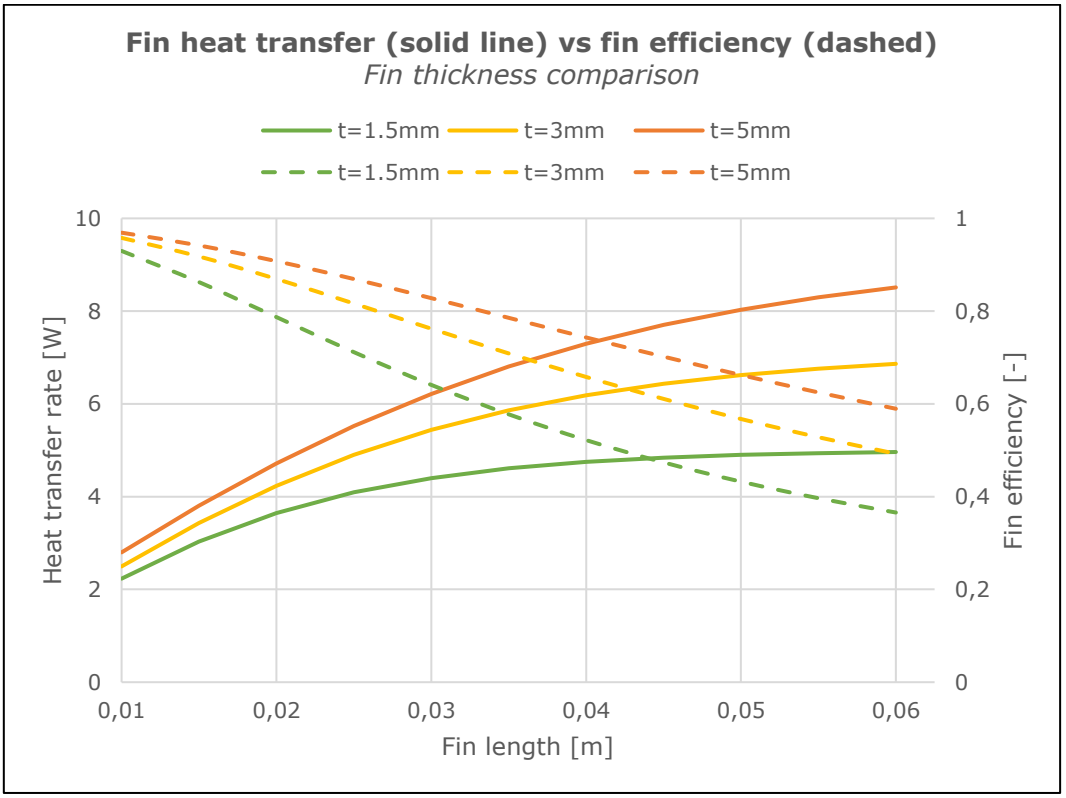


**Figure 5-2:** Fin heat transfer rate vs fin efficiency

Fig. 5-2 shows that the fins get less efficient with increasing length while the heat transfer from the fin increases, due to the fin area gets larger. Note that for a fin length of 60 mm, the heat transfer rates converge, as the fin efficiency drops. This also corresponds with the converging fin tip temperature in fig. 5-1. Also, increasing the fin thickness makes the fins more efficient, resulting in larger heat transfer rate.

In other words, increasing the fin thickness leads to larger heat transfer to the pcm, which means faster melting and more heat stored. On the other hand, the increased thickness also adds weight to the system and displaces the pcm. Though the fins also pose sensible heat storage, the main goal for the concept is to store latent heat to reduce system weight and size, making the LHS unit appear more compact.

However, the heat transfer magnitude is rather small and as the system weight is a key issue, the heat transfer from the fin should be compared to its weight. This was done by defining the fin performance factor $C_f$ given by eq. *(5.7)*, which is the heat transfer rate relative to the fin weight. The results are shown in fig. 5-3.

$$C_f = \frac{q_f}{m_{fin}} = \frac{q_f}{\rho_{steel} A_c L_f} \qquad \left[\frac{W}{kg\ fin}\right] \tag{5.7}$$

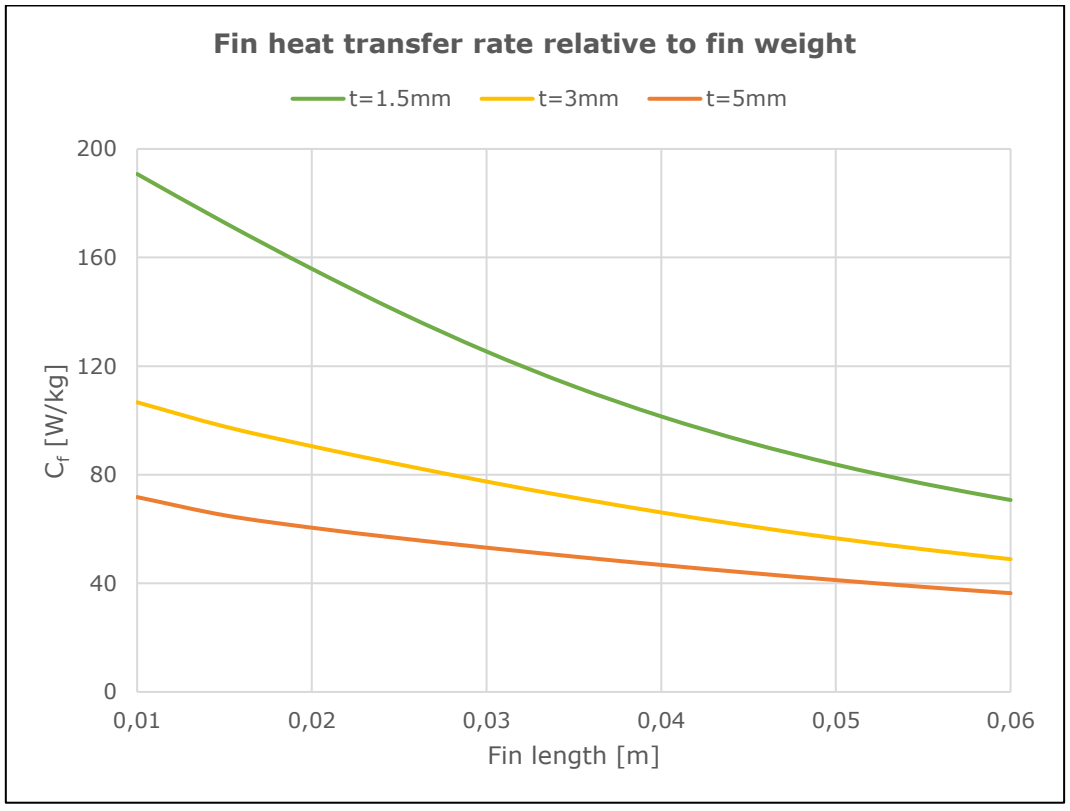


**Figure 5-3:** Heat transfer rate from fin relative to its weight

As the increase in fin thickness leads to larger heat transfer, this difference is rather small compared to the increased weight this entails, as seen in fig. 5-3. Hence, a fin thickness of 1.5 mm has the best performance for this parameter ($C_f$), e.g. for a fin length of 60 mm, increasing the thickness to 3 mm, the heat transfer increases with 30 % while the weight increases with 50 %. Thus, increasing the thickness leads to worse performance.

## 5.2 Proposal for new container design

Based on the fin analysis, a proposed fin arrangement in the container is presented in this chapter, which will be beneficial to increase the heat transfer in the pcm. As it is desirable to both achieve faster melting and at the same time keeping the LHS unit weight low, a compromise has been selected by setting the fin thickness to 3 mm. Regarding the fin efficiency, the design point of 10°C difference between the fin tip and the surrounding pcm, then gives a bottom fin length of 50 mm as seen in fig. 5-1. This way, the fin tip will also contribute to heat transfer.

For the top fins, similar temperature development in the fins is expected. However, the driving forces (temperature difference) between the pcm and the fin base are smaller during discharge. This can be seen in fig. 4-13 where the heat loss gradient is gentler when compared to charge. Hence, the top fin length can be somewhat larger, e.g. 70 mm. Also note that $T_b<T_\infty$ for the top fins, as the pcm now is the hot side.

In other words, the bottom fins will lose heat faster due to larger temperature difference between bottom and pcm, whereas the top fins will receive less heat from the pcm, such that their length can be increased and still be efficient.

Table 5.3 lists the selected fin dimensions and its performance, whilst a 3D model of the new design is shown in fig. 5-4. The angles between the fins are set such that the thermocouples can be placed at the same position as for the base case design (dashed line), for comparison of the results.

**Table 5.3** – Selected fin arrangement parameters

| | **Bottom** | **Top** | **Unit** |
|---|---|---|---|
| Number of fins, *N* | 4 | 4 | - |
| Fin width, *w* | 100 | 100 | mm |
| Fin length, $L_f$ | 50 | 70 | mm |
| Fin thickness, *t* | 3 | 3 | mm |
| Heat transfer, $q_f$ | 6.6 | - | W |
| Fin efficiency, $\eta_f$ | 56.7 | - | % |

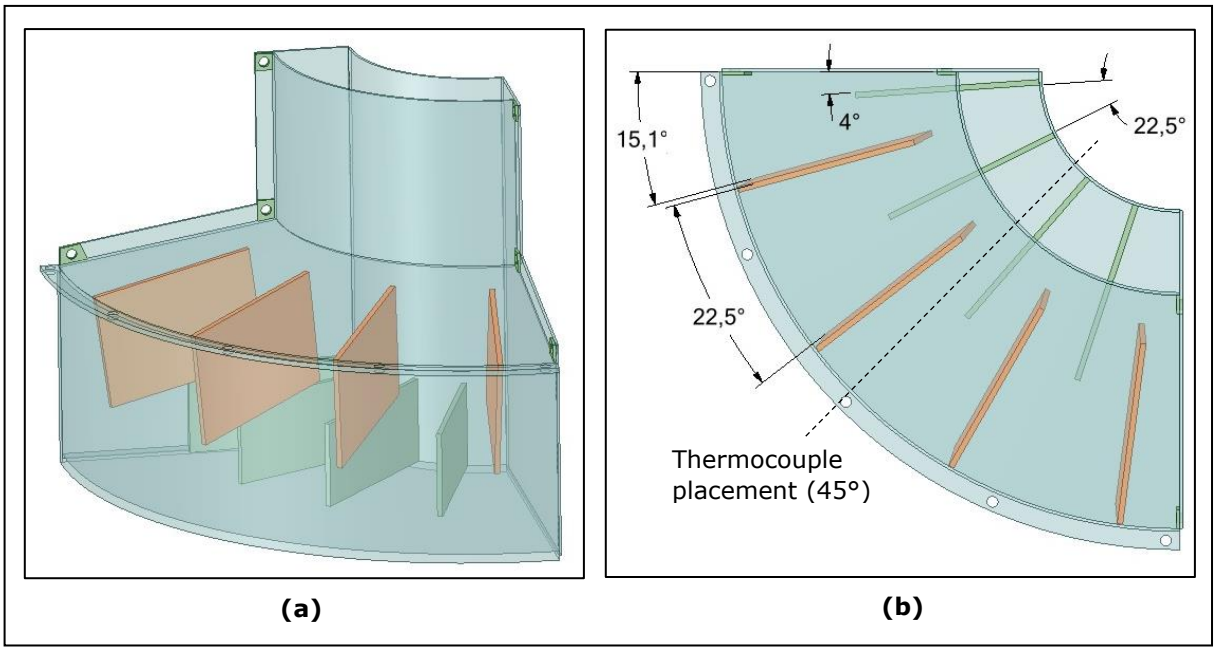


**Figure 5-4:** Proposed fin design; (a) 3D model of container with internal fins; (b) top view of container showing fin configuration

Note that due to the simplified analysis, which is based on steady state, a 3D numerical simulation should be done to get a better understanding of the fin performance, as the heat transfer is transient. Then necessary adjustments can be done before producing a new container for testing.

Alternatively, perhaps using metallic foam as HTE is a better choice with respect to the system weight. As seen in fig. 5-3, the shorter the fin length, the better the performance factor $C_f$ is.

In addition, the largest thermal resistance for the concept is probably on the container outside, due to the small heat transfer coefficient to air, which will limit the heat loss during discharge. Hence, some HTE measures should be considered for the outside wall as well. On the other hand, it should compromise with the design, as the aesthetics of the LHS unit likely is as important as its thermal performance, to meet customer expectations.

# 6 CONCLUSION AND FURTHER WORK

The purpose of this Master thesis was to experimentally test a compact, passive and durable latent heat storage (LHS) unit to be integrated on wood stoves. The concept is imagined placed on the stove top and consists of a coaxial container wrapped around the stove pipe, filled with high-density polyethylene (HDPE) which will act as a phase change material (PCM). Due to the phase change, latent heat is stored in the material, thus higher energy density and lower weight can be achieved for the unit, when compared to traditional solutions with only sensible heat storage, e.g. soapstone. The aim was to store substantial part of the peak effects during batch combustion, resulting in a more stable heat release to the room and further improved thermal comfort.

The concept was based on the previous project work [7] and its geometry was slightly changed to achieve better heat transfer to the room and make it more compact. It was assumed that a 90-degree slice of the concept would be sufficient to study the heat transfer in the PCM. The container material was also changed from aluminium to stainless steel, due to practical reasons. During the experimental design, the container height was reduced by half, as the desired heat load could not be applied. However, this was later resolved. To simulate the heat flow from the wood stove top, a heat cable was inserted into a custom-made heating plate of pure copper to achieve uniform heating of the container bottom.

The main challenge regarding the design was to facilitate fast melting (storing latent heat) and slow solidification (heat release after combustion) for a reasonable combustion duration, and at the same time keeping the max temperature in the PCM below its degradation point, as this would deteriorate the material and affect the thermal performance of the concept. Preliminary testing was carried out to test the potential oxidation of HDPE, as the combination of heat and oxygen was a known issue which would influence its properties.

Further, thermal degradation was avoided by temperature control in the heating plate, using a control system to regulate the heat load. Thermocouples were used to log temperatures in the PCM and the test rig was properly insulated to achieve a reasonable heat balance. The fresh HDPE was in form of shavings and proved time-consuming to melt such that the desired amount of PCM could be filled into the container. Hence, the primary test was run with only half-full container. Nevertheless, it was assumed to be a good demonstration of the concept.

The primary test consisted of two different cycles, one which was completely insulated (C1) while the other was semi-insulated (C2), as the outer side wall insulation was removed. Hence, the C2-cycle can be viewed as the demonstration of the concept, as the final LHS unit has no insulation. Several parameters were analysed, including temperature development, phase change front, heat balance and thermal conductivity. Uncertainties were also evaluated.

Due to more heat loss during C2, the PCM average temperature was lower at charge end, the melting was slower and the solidification was faster. Note that the phase change process was tracked only at the core of the material, due to limited measuring points. There were large temperature differences within the PCM for both test cycles, indicating that free convection was absent, as the convective effect would result in more consistent temperatures, expectedly.

The heat balance for the test rig was used to estimate the heat stored in the PCM, which then was compared to the enthalpy change in the PCM, to verify the values. Although the values were somewhat different, likely due to simplifications in the method, the gap could be explained by uncertainty for C2. For further validation of the results, the effective thermal conductivity was estimated, which proved similar to literature values, which in turn supported the assumption of only conduction heat transfer in the PCM.

For C2, the PCM stored approx. 0.4 kWh at charge end, such that it would store 3.2 kWh when scaled up to the final concept, assuming similar temperature development. This is about half of the desired heat to store. However, the heating plate posed a large thermal mass with sensible heating, storing significant parts of the heat load. Due to its temperature control, the heat load rapidly decreased when setpoint was reached. This proved to be a weakness in the experimental design, as part of the goal was to test the concept for max heat flux to the container bottom.

Further, heat transfer enhancement (HTE) can help to increase the heat stored in the PCM, especially due to the absence of free convection. Assumingly, this would also result in faster melting and better distribution of the heat flow in the PCM, reducing the risk of degradation in the bottom layer. A brief fin analysis was then carried out to propose a new container design for future testing, consisting of 8 alternating radial fins from the container bottom and top. As the analysis was rather simple, it is noted that 3D simulation of the fin design should be done to better understand its thermal performance, as the heat transfer is transient. Alternatively, other HTE methods can be considered, e.g. metallic foam, especially with respect to the system weight.

List of proposals for further work:

- Complete filling of container in base case for a new test
- Improve instrumentation (calibrate thermocouples, add heat flux sensors for better estimation of heat loss)
- Test new design using HTE (fins or metallic foam) for comparison
- Numerical simulation of current test rig for comparison and validation of the phase change front; only transient conduction due to absence of free convection
- Measure HDPE properties (especially latent heat and dynamic viscosity) to improve accuracy of calculations and numerical model
- Test the concept using other PCMs (e.g. erythritol) with lower viscosity such that free convection can be achieved

# 7 REFERENCES


[1] https://energifaktanorge.no/norsk-energibruk/energibruken-i-ulike-sektorer/#husholdninger (webpage, Norwegian Ministry of Petroleum and Energy)

[2] http://norskvarme.org/fakta-om-vedfyring/ (webpage, Norwegian trade association for fireplaces)

[3] L. Georges, Ø. Skreiberg, V. Novakovic, *On the proper integration of wood stoves in passive houses under cold climates,* Energy and Buildings 72, 2014, p. 87-88

[4] A. Sharma, V. V. Tyagi, C. R. Chen, D. Buddhi, *Review on thermal energy storage with phase change materials and applications,* Renewable and Sustainable Energy Reviews, 2009, vol. 13, p. 318-345

[5] A. Sevault, H. Kauko, M. Bugge, K. Banasiak, N. E. Haugen, *Phase change materials for thermal energy storage in low and high temperature applications: a state-of-the-art,* SINTEF Energy Research, 2017, p. 5-24

[6] A. Sevault, J. Soibam, N. E. Haugen, Ø. Skreiberg, *Investigation of an innovative latent heat storage concept in a stovepipe,* Chemical Engineering Transactions, 2018, vol. 65, p. 25-30

[7] H. Mathisen, *Numerical analysis of heat transfer in phase change materials for thermal energy storage*, Department of Energy and Process Engineering, NTNU, 2019, project work

[8] C. Zauner, F. Hengstberger, M. Etzel, D. Lager, R. Hofmann, H. Walter, *Experimental characterization and simulation of a fin-tube latent heat storage using high density polyethylene as PCM*, Applied Energy, 2016, vol. 179, p. 237-246

[9] J. Gasia, M. Martin, A. Solé, C. Barreneche, L. Cabeza, *Phase change material selection for thermal processes working under partial load operating conditions in temperature range between 120 and 200 °C*, Applied Sciences, 2017, vol. 7, p. 722

[10] A. Safari, R. Saidur, F. A. Sulaiman, Y. Xu, J. Dong, *A review on supercooling of phase change materials in thermal energy storage systems,* Renewable and Sustainable Energy Reviews, 2017, vol. 70, p. 905-919

[11] R. Al-Shannaq, J. Kurdi, S. Al-Muhtaseb, M. Dickinson, M. Farid, *Supercooling elimination of phase change materials (PCMs) microcapsules*, Energy, 2015, vol. 87, p. 654-662

[12] K. S. Ytredal, *Investigation of heat storage in future wood stoves,* Department of Energy and Process Engineering, NTNU, 2015, Master thesis

[13] J. Yang, L. Yang, C. Xu, X. Du, *Experimental study on enhancement of thermal energy storage with phase-change material,* Applied Energy, 2016, vol. 169, p. 164-176

[14] *HDPE material properties database file,* shared by A. Sevault, SINTEF Energy Research

[15] Ø. Skreiberg, L. Georges, *Transient heat production and release profiles for wood stoves,* Chemical Engineering Transactions, 2018, vol. 65, p. 223-228

[16] K. Kristjansson, E. Næss, Ø. Skreiberg, *Dampening of wood batch combustion heat release using phase change material heat storage: Material selection and heat storage property optimization,* Energy, 2016, vol. 115 part 1, p. 378-385

[17] https://durathermfluids.com/products/duratherm-630/ (webpage, technical data sheet)

[18] https://www.engineeringtoolbox.com/material-properties-t_24.html (webpage)

[19] https://www.pettersen.no/produkter/h-900c-varmekabler/ (webpage, heat cable supplier)

[20] *3D model of heating plate*, designed and shared by Senior engineer Håvard Rekstad, Department of Energy and Process Engineering, NTNU

[21] F. P. Incropera, D. P. Dewitt, T. L. Bergman, A. S. Levine, *Incropera's principles of heat and mass transfer,* Wiley & Sons Inc, 2017, Appendix A

[22] F. P. Incropera, D. P. Dewitt, T. L. Bergman, A. S. Levine, *Incropera's principles of heat and mass transfer,* Wiley & Sons Inc, 2017, Chapter 9.6

[23] https://en.wikipedia.org/wiki/Ziegler-Nichols_method (webpage)

[24] J. G. Ziegler, N. B. Nichols, *Optimum settings for automatic controllers,* Transactions of the ASME, 1942, vol. 64, p. 759-768

[25] F. P. Incropera, D. P. Dewitt, T. L. Bergman, A. S. Levine, *Incropera's principles of heat and mass transfer,* Wiley & Sons Inc, 2017, Chap. 3.6, p. 143-163

[26] R. J. Moffat, *Describing the uncertainties in experimental results*, Experimental Thermal and Fluid Science, 1988, vol. 1, p. 3-17

# APPENDICES

A: HDPE properties

B: Thermocouples calibration attempt

C: Uncertainty analysis

D: Risk assessment

## Appendix A: HDPE properties

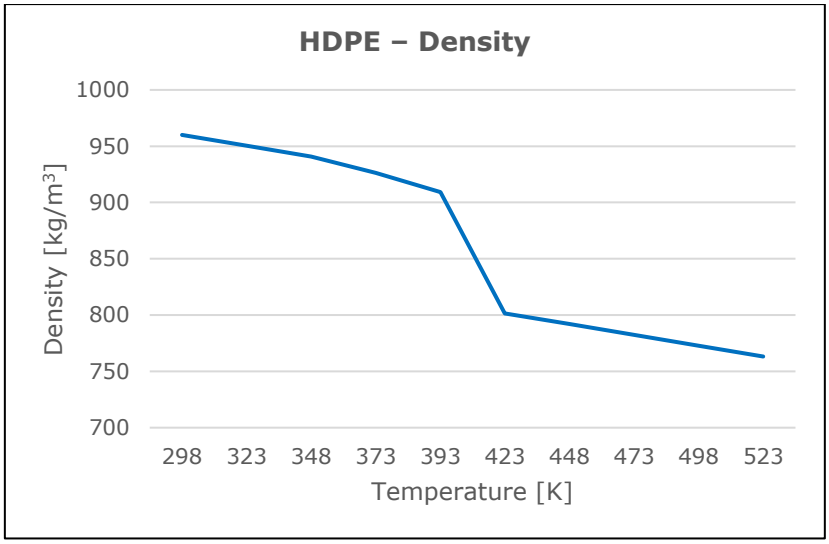


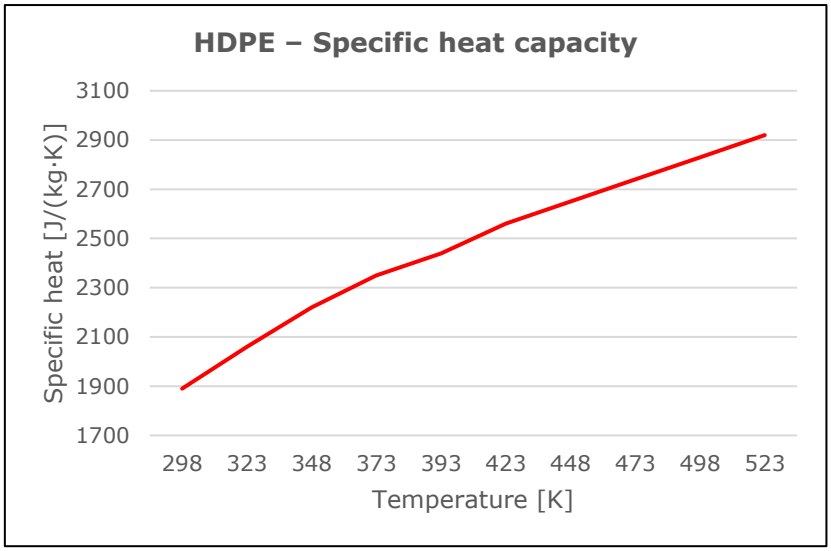


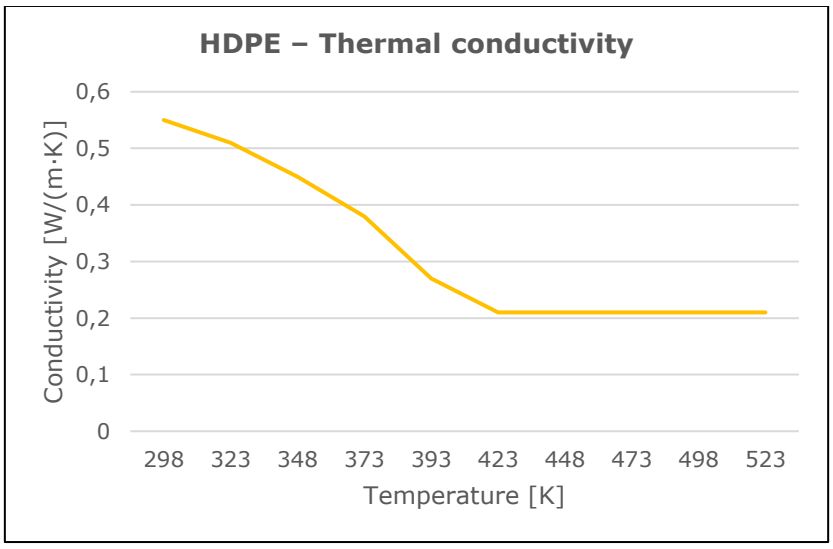

## Appendix B: Thermocouples calibration attempt

The thermocouples used in the experiment are type K elements, with a typical accuracy of ± 2.2 K, and calibration was planned to achieve more precise measurements. However, the laboratory calibrator was sent away for calibration itself, so a simple method using water as reference was carried out. A slush of ice-water was used for 0°C and boiling water for 100°C.

In general, the boiling point for water is 100°C at standard atmospheric pressure (1.013 bar). Specifically, it is a function of pressure and the following approach was done to determine the current boiling point. Due to that no barometer was found in the lab, the atmospheric pressure was taken from meteorological measurements that day to be 1.016 bar. Further, it was assumed that the air pressure in the lab room was the same as the outside air pressure, but due to ventilation, it was reduced by 2 %. The boiling point was then calculated based on the August equation *(b.1)*, where the pressure unit is millimetre of mercury, mmHg.

$$p[mmHg] = \exp\left(20.386 - \frac{5132}{T[K]}\right) \qquad (b.1)$$

Equation *(b.1)* expresses an approximation of the linear relation between logarithmic vapor pressure and the coherent temperature. For unit conversion; 1 bar equals $10^5$ Pa, 1 mmHg is 133.32 Pa, so the air pressure is then 762.08 mmHg. Considering the assumed pressure drop due to ventilation, the pressure is 746.84 mmHg. From equation *(b.1)*, the temperature is then 372.7 K or 99.5 °C. It should be mentioned that impurities in the water also would affect its boiling point, but this was disregarded.

**Table B.1** – Thermocouples calibration data

| | ***Ice water (0 °C)*** | | ***Boiling water (99.5 °C)*** | |
|---|---|---|---|---|
| | Measured value | Deviation | Measured value | Deviation |
| TC00 | 0.3 | 0.3 | 98.1 | -1.4 |
| TC01 | 0.2 | 0.2 | 97.9 | -1.6 |
| TC02 | 0.5 | 0.5 | 98.3 | -1.2 |
| TC03 | 0.6 | 0.6 | 98.1 | -1.4 |
| TC04 | 0.4 | 0.4 | 98.2 | -1.3 |
| TC05 | 0.1 | 0.1 | 98.2 | -1.3 |
| TC06 | 0.3 | 0.3 | 98.4 | -1.1 |
| TC07 | 0.3 | 0.3 | 98.3 | -1.2 |
| TC08 | -0.1 | -0.1 | 98.3 | -1.2 |
| TC09 | 0.3 | 0.3 | 98.3 | -1.2 |
| TC10 | 0.5 | 0.5 | 98.3 | -1.2 |
| TC11 | -0.1 | -0.1 | 98.3 | -1.2 |
| TC12 | 0.1 | 0.1 | 98.3 | -1.2 |
| TC13 | -0.1 | -0.1 | 98.3 | -1.2 |
| TC14 | -0.2 | -0.2 | 98.2 | -1.3 |
| *Average value:* | | *0.2* | | *-1.3* |

Table B.1 shows the measured temperature for each thermocouple and the deviation from the reference point. These data were supposed to form the basis for the calibration, but due to the simplified method, the deviation seemed to become unreasonable for increasing temperature.

Hence, the calibration data should include a set of values for a higher temperature to cover the range during the experiment, e.g. by using a heated bed. Instead, a linear regression based on the average deviation for each point, was done:

$$y = ax + b$$

$$T(calibrated) = \frac{98.2 - 0.2}{99.5 - 0} T + 0.2$$

Where *T(calibrated)* is the TC temperature and *T* is the actual temperature. The pcm was expected to reach 250°C at maximum, so the average calibrated measurement would be 246.5°C at this point, thus 3.5°C below the actual temperature, which is larger than the given accuracy for type K elements (± 2.2°C). In other words, this calibration method would risk making the TC worse compared to keeping them non-calibrated. Further, it seemed unlikely that the deviation would be that large at this point, as the TC are applicable for temperatures up to 1100°C.

Thus, calibration was omitted for the experiment due to the simplified method with a somewhat uncertain value used for the boiling point. However, the absolute uncertainty for type K elements is small compared to the large temperature range experienced by the pcm. The uncertainty analysis if further discussed in Appendix C.

## Appendix C: Uncertainty analysis

The uncertainty analysis is based on the procedure described by Moffat [26], where the purpose is to estimate the effect that measurement uncertainties have on the calculated result.

For a variable $X_i$ with a known uncertainty $\Delta X_i$, the variable with its uncertainty can be expressed as:

$$X_i = X_i(measured) \pm \Delta X_i \qquad (c.1)$$

Equation *(c.1)* can be understood as the *measured value* $X_i$ is the best estimate for $X_i$ and that there is an uncertainty that may be as large as $\pm\Delta X_i$.

Further, the calculated result from the measurements of the experiment, $R$, will have an uncertainty, $\Delta R$, such that:

$$R = R(X_1, X_2, X_3, \dots, X_n) \pm \Delta R \qquad (c.2)$$

where the uncertainty in the measured values used in the calculation of R, will affect the uncertainty of the result, which can be estimated by the root-sum-square method of the individual uncertainties:

$$\Delta R = \left[\sum_{i=1}^{n} \left(\frac{\partial R}{\partial X_i}\Delta X_i\right)^2\right]^{1/2} \qquad (c.3)$$

Each term in equation *(c.3)* represents the contribution by the uncertainty of a variable, to the uncertainty of the result, assumed that the individual uncertainties are independent of each other.

The experimental data consists of single-sample measurements, as none of the values were measured more than once for the same point during the process. In addition, modifications were done between the tests performed (side wall insulation removed), thus the conditions were not the same.

Further, assuming a Gaussian distribution for the measured value $X_i$ (temperature), the uncertainty $\Delta X_i$ (2.2 K) represents two standard deviations from the nominal value, with a probability of 1 out of 20 that the value is outside the uncertainty. This implies that when repeating the experiment, the measured values are expected to be within the same range in 95 % of the tests [26].

The individual uncertainties used to estimate the uncertainty of the results, are listed in Table C.1. Due to the simple calibration method, which was not implemented, the typical uncertainty for type K thermocouples was used. The TC position uncertainty is based on possibly inaccurate mounting of the cannula pipes and further influence by forces in the PCM (e.g. phase change contraction or convection), although the pipes that reach the farthest into container volume were reinforced with a steel bracket to avoid any movement. The TC position is further used to calculate the *VF* (volume fraction melted), in addition with the filling level, which is based on a visual estimate.

The HDPE and thermal oil were weighed for several batches using a simple kitchen scale, so the uncertainty for the PCM mass is an assumption. The material properties of HDPE were not measured, but theoretical, so its uncertainties were disregarded. However, for the insulation materials, consistent values for specific heat were difficult to find, thus the large uncertainty listed. The insulation surface area was calculated from dimensions measured by using a ruler, so somewhat uncertain. The uncertainty in mass of the other components were based on the volume and density of the respective material, which also were inaccurate.

Finally, regarding the heat load, there was most likely some changes in voltage during the test and a relative uncertainty was assumed (probably larger than 2 %; P=VI, where V perhaps varies with 5-10 % due to other lab activities).

Also, the listed uncertainties in Table C.1 are of different types, e.g. for the thermocouple (random error, all TC are probably from the same batch) opposed to thermocouple position (fixed error, used ruler to measure distance).

**Table C.1** – Individual uncertainties

| **Variable** | **Uncertainty** |
|---|---|
| Non-calibrated TC (type K) | ± 2.2 K |
| TC position | ± 1 mm |
| Filling level | ± 5 mm |
| PCM mass | ± 0.1 kg |
| Insulation surface area | ± 0.01 $m^2$ |
| Cu/stainless steel mass | ± 0.1 kg |
| Insulation materials, $c_p$ | ± 100 J/kg·K |
| Insulation materials, mass | ± 0.1 kg |
| Heat load (heat cable power) | ± 2 % |

As an example, the following calculation shows how the uncertainty of the average temperature is found:

$$T, av = \frac{\sum_{i=1}^{n} T_i}{n} = \frac{T_1 + \cdots + T_6}{6}, \quad n = 6$$

$$\frac{\partial T, av}{\partial T_i} = \frac{1}{6}$$

$$\Delta T, av = \left[6 \cdot \left(\frac{1}{6} \cdot 2.2\ K\right)^2\right]^{1/2} = 0.9\ K$$

The uncertainties listed in Table C.2 are based on eq. *(3.3)* for heat stored, eq. *(3.4)-(3.6)* for heat loss and further calculated using the individual uncertainties from Table C.1 and the nominal values for the respective variable.

**Table C.2** – Uncertainties for calculated results of heat balance at charge end

| **Variable** | **C1** [kWh] | **C2** [kWh] |
|---|---|---|
| ΔQ,input | ± 0.028 | ± 0.032 |
| ΔQ,heating plate | ± 0.005 | ± 0.005 |
| ΔQ,container | ± 0.004 | ± 0.004 |
| ΔQ,insulation | ± 0.013 | ± 0.010 |
| ΔQ,loss air | ± 0.003 | ± 0.006 |
| ΔQ,loss table | ± 0.001 | ± 0.001 |
| ΔQ,pcm (heat balance) | ± 0.032 | ± 0.035 |

When using the test rig heat balance to estimate heat stored in the pcm, *Q,pcm* is calculated from *Q,in* minus the combined heat loss and heat stored in the other components. Further, *ΔQ,pcm* is the root-sum-square of all the calculated uncertainties for each component, according to equation *(c.3).*

For the stored heat in components, the uncertainty is calculated based on individual uncertainties. For the heat loss (which is a heat transfer rate), first the uncertainty of the heat loss at charge end is calculated and then changed to kWh during one min of flow time, assuming stable heat loss for each minute. This uncertainty is further used to find the combined uncertainty for the entire amount of heat loss during charge, by the root-sum-square method.

Note that the absolute uncertainty, *ΔQ,in*, for C2 is larger than for C1, due to larger *Q,in* during the semi-insulated cycle (C2) and assumed same relative uncertainty as listed in Table C.1. Further, the uncertainty for heat stored in the insulation is slightly smaller for C2 (semi-insulated) due to less insulation, hence the individual uncertainty of the insulation mass makes less impact. On the other hand, the uncertainty for heat loss to air is larger for C2, as radiation becomes a part of the equation.

The uncertainty of the control calculation for heat stored in the PCM, *ΔQ,pcm*, is based on eq. *(4.2)*, using the average temperature listed in Table 4.3, material properties from Table 3.1 and the uncertainties in Table C.1 and C.3.

**Table C.3** – Uncertainties for calculated results to estimate heat stored in PCM at charge end

| **Variable** | **C1** | **C2** |
|---|---|---|
| ΔT,av (pcm average T) | ± 0.9 K | ± 0.9 K |
| ΔVF (melt front) | 0 % | 7.6 % |
| ΔQ,pcm (control) | ± 0.021 kWh | ± 0.022 kWh |

*ΔT,av* is calculated from the individual uncertainty for each thermocouple, where it is more likely that the error for each single measurement would cancel each other out for the average value. Hence, *ΔT,av* is smaller than the individual TC uncertainty (2.2 K).

The uncertainty of the melting front *ΔVF* is calculated based on eq. *(4.1)* and the individual uncertainties of TC placement and container filling level, e.g. when T1>melt temp, the volume below its position is melted and so on. The accuracy is also dependent on TC accuracy, but for C1 all temperatures were well above melting point and a visual check confirmed that the PCM was completely melted. For C2, some PCM in the top layer was not melted, thus melting could only be assumed up to T3-position.

The uncertainties of the thermal conductivity are listed in Table C.4 and were calculated based on eq. *(4.5)* and the values listed in Table 4.6 for each position of the respective thermocouple.

**Table C.4** – Uncertainties of effective thermal conductivity at charge end

| | **C1: insulated** | | **C2: semi-insulated** | |
|---|---|---|---|---|
| **TC position** | Absolute [W/m·K] | Relative [%] | Absolute [W/m·K] | Relative [%] |
| T1 | ± 0.04 | ± 12.1 | ± 0.03 | ± 13.6 |
| T2 | ± 0.02 | ± 4.2 | ± 0.02 | ± 5.9 |
| T3 | ± 0.02 | ± 3.8 | ± 0.01 | ± 2.6 |

The absolute uncertainties for C2 are smaller than for C1, probably due to more stable temperature gradients (fig. 4-16) at charge end (larger heat loss for C2), thus there is less heating of the PCM during C2 compared to C1. Hence, more of the heat is flowing through the PCM and gives a better estimate for the thermal conductivity. In other words, C2 is closer to steady state at charge end, where the heat balance is stable (q,in=q,out) and heat only flows through PCM without increasing the temperature.

If the temperature gradient is steep, the heat flow from container bottom is heating the PCM, opposed to if the gradient is gentle (more stable temperature) where the heat flow is through the pcm – which is the best condition to estimate thermal conductivity.

Also note that the uncertainty is lower for T3 position, as the individual uncertainty of both TC position and temperature is less important due to smaller relative uncertainty (both distance for thermal resistance and temperature difference is larger).

In addition, the real heat flow in the pcm is three-dimensional and is also affected by the container side walls. Including the larger heat loss during C2, it complicates the heat balance further. However, due to the heat load was evenly distributed in the heating plate, a uniform heat flow to the container bottom and then through the pcm layers can be expected. For the estimation method of thermal conductivity, this makes it reasonable to assume one-dimensional heat flow/conduction in the pcm.

## Appendix D: Risk assessment

To evaluate the technical safety of the laboratory test rig, a Hazard and operability study (HAZOP) was carried out. Figure D-1 shows the experimental set-up before it was insulated (to better show the elements which were evaluated) and the corresponding ID numbers of each element in the risk assessment form.

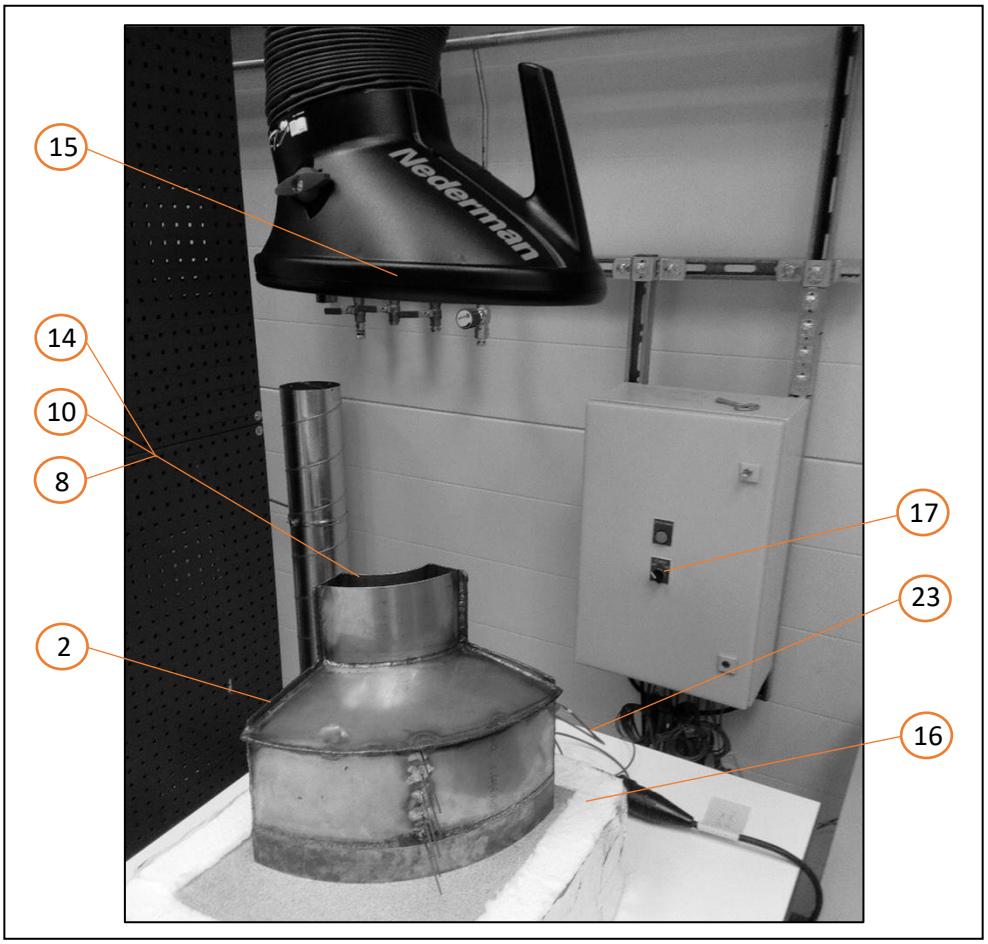


**Figure D-1:** Experimental set-up with corresponding ID numbers

Further, each element in the risk assessment form is evaluated using a colour code mark, where green indicates an acceptable risk. The letters and numbers in the marks indicates the severity of consequences and probability, respectively. All elements have been rated with low-to-medium probability and with small consequences.

**Evaluation (in Norwegian) follows on the two next pages:**

# HAZID/HAZOP av

| | |
|---|---|
| Prosjektnummer/-navn | 502001554 |
| Prosjektleder | Alexis Sevault |
| Labsjef | Helen Langeng |
| Forskningsleder | Line Rydså |
| Forskningssjef | Petter E. Røkke |
| Ansvarlig operatør | Alexis Sevault |
| Vurdering utført av | Alexis Sevault, Henning Hvål Mathisen og Helen Langeng |

Dato, sign Prosjektleder 24. juni 2019 - Alexis Sevault

Dato, sign Labsjef 25/6-19 - Helen Langeng

Dato, sign Forskningsleder 28/6-19 Line Rydså

Dato, sign Forskningssjef 28/6-19

SINTEF

**Enhet:** SINTEF Energi AS
**Bygning:** VATL, NTNU
**Rom eller rigg / utstyr:** Rom C114 / PCM-LAB

**Dato:** 2019-06-18
**Deltagere:** Alexis Sevault, Henning Hvål Mathisen og Helen Langeng
**Linjeleder:** Petter Røkke

| Id | Aktivitet | Mulig hendelse | Mulig konsekvens | Eksisterende barrierer | Risikoverdi med eksisterende tiltak | | | | Nye barrierer / risikoreduserende tiltak (handlingsplan) | Risikoverdi med nye tiltak | | | | Ansvarlig Frist | Status |
|---|---|---|---|---|---|---|---|---|---|---|---|---|---|---|---|
| | | | | | Menneske | Ytre miljø | Omdømme | Økonomi / materiell | | Menneske | Ytre miljø | Omdømme | Økonomi / materiell | | |
| 1 | Forsøket som skal gjennomføres består av en testrigg der det skal smeltes HDPE i en container av rustfritt stål som er plassert på en varmeplate av kobber m/varmekabel. Fase 1 er tenkt som en grunntest der all HDPE smeltes og deretter størknes ved at effekten på varmekabelen skrus av. Temperaturer i HDPE måles gjennom forløpet | | | | | | | | | | | | | | |
| 2 | Ingen strømning/No flow | Ekspandering av HDPE under oppvarming | Lekkasje | Lokk sveises igjen | v | v | v | A3 | | | | | | | |
| 8 | Høyere trykk/More pressure | Container åpent system | Ingen trykkøkning | Åpning i topp | v | v | v | v | | | | | | | |
| 10 | Høyere temperatur/More temperature | Lekkasje toppåpning olje/HDPE, smeltepunkt HDPE: T=132 grader C | Brannskade hud | Verneutstyr (hansker, frakk, vernebriller) | B2 | v | v | v | | | | | | | |
| 14 | Endring i sammensetning/Composition Change | Urenheter i olje, rask koking | Sprut fra toppåpning | Verneutstyr, avstand fra rigg, strømbryter på el-skap skrus av | B2 | v | v | v | | | | | | | |
| 15 | Forurensning/Contamination | Avgasser fra HDPE/olje | Ikke giftig eller miljøskadelig, men uheldig ved innånding/pust | Punktavsug over rigg | A3 | v | v | v | | | | | | | |
| 16 | Lekkasje/ leakage | HDPE/olje lekkasje | Søl på resten av rigg/isolasjon, kontakt med hud | Verneutstyr | A1 | v | v | A3 | | | | | | | |
| 17 | Instrumentering/Instrumentation | Feil; termoføler, varmekabel, elektrisk anlegg, PC-krasj | Ingen temperaturkontroll, ødelagt utstyr, ødelagt forsøk | Strømbryter på el-skap skrus av | A1 | v | v | A1 | | | | | | | |
| 23 | Antennelse/Ignition | Flash point for olje, 229 grader C | Flammebluss, antennelse i HDPE | Temperaturkontroll på den eneste varmekilden. Ingen tennkilde i nærheten. | B1 | v | v | A3 | | | | | | | |
| 28 | | | | | | | | | | | | | | | |
| 29 | | | | | | | | | | | | | | | |
| 30 | | | | | | | | | | | | | | | |
| 31 | | | | | | | | | | | | | | | |
| 32 | | | | | | | | | | | | | | | |
| 33 | | | | | | | | | | | | | | | |
| 34 | | | | | | | | | | | | | | | |
| 35 | | | | | | | | | | | | | | | |
| 36 | | | | | | | | | | | | | | | |
| 37 | | | | | | | | | | | | | | | |
| 38 | | | | | | | | | | | | | | | |
| 39 | | | | | | | | | | | | | | | |
| 40 | | | | | | | | | | | | | | | |

NTNU
Norwegian University of
Science and Technology